

A New Tool for Detecting BSM Physics in $B \rightarrow K^* \ell \ell$ Decays

A. SIBIDANOV¹, T. E. BROWDER¹, S. DUBEY¹, S. KOHANI¹, R. MANDAL²,
S. SANDILYA³, R. SINHA^{4,1}, AND S. E. VAHSEN¹

¹*University of Hawai‘i at Manoa, Honolulu, HI 96822, USA*

²*Center for Particle Physics Siegen (CPPS), Universität Siegen, 57068 Siegen, Germany*

³*Indian Institute of Technology Hyderabad (IITH), Telangana 502285, India*

⁴*The Institute of Mathematical Sciences (IMSc), Taramani, Chennai 600113, India*

ABSTRACT

Flavor-changing neutral current (FCNC) processes such as $b \rightarrow s \ell \ell$ do not occur at tree-level in the Standard Model (SM), which makes them sensitive probes of physics beyond the standard model (BSM). Intriguing BSM hints in $b \rightarrow s$ transitions have been observed by multiple flavor physics experiments, LHCb, Belle, BaBar, and Belle II. We have upgraded the widely used event generator `EvtGen` to model $B \rightarrow K^* \ell^+ \ell^-$ with improved SM decay amplitudes and amplitudes for possible BSM physics contributions, implemented in the operator product expansion in terms of Wilson coefficients; this upgraded event generator can then be used to investigate the experimental sensitivity to the most general BSM signal resulting from dimension-six operators. We describe the advantages and potential of the newly developed ‘Sibidanov Physics Generator’ in improving sensitivity of searches and clarifying signatures. Advantages include properly simulating BSM scenarios, interference between SM and BSM amplitudes, and correlations between different BSM observables as well as acceptance bias. We show that exploiting such correlations substantially improves experimental sensitivity. As a demonstration of the proposed approach, we review the prospects for improved measurements with $B \rightarrow K^* \ell \ell$ decays from the expected 50 ab^{-1} dataset of the Belle II experiment with a four-dimensional unbinned maximum likelihood fit. We describe new promising experimental signatures, and novel ideas such as Δ -observables, which reduce uncertainties in the SM expectations due to QCD and resonance effects. The Δ -observables appear ideally suited for Belle II with the large data sets expected in the next decade. Belle II also has excellent sensitivity to New Physics (NP) in the Wilson coefficients C_7 and C'_7 , which appear at low q^2 in the di-electron channel.

Contents

1	Executive summary	3
2	Overview	4
2.1	Current experimental anomalies in $b \rightarrow s$ neutral current (FCNC) processes	4
2.2	Definition of observables and angular asymmetries	5
2.3	SM and candidate NP possibilities and their Lorentz structures	6
2.4	Form factor uncertainties	7
2.5	Modifications to the EvtGen Monte Carlo Generator	9
3	Signatures of NP in $B \rightarrow K^* \ell^+ \ell^-$ and improved sensitivity via multi-dimensional likelihood fits	11
3.1	δC_9 correlated signatures in A_{FB} and S_5 (and $d\Gamma/dq^2$)	11
3.2	δC_{10} sensitivity	13
3.3	C'_9 and C'_{10} sensitivity	14
3.4	C_7, C'_7 signatures at low q^2 and in the χ angle distribution	15
4	How to disentangle QCD and resonance effects from NP in $B \rightarrow K^* \ell^+ \ell^-$	19
5	Description of the theoretical framework	24
6	Signal generator performance improvements	27
7	Future work	28
7.1	Full MC simulation and EvtGen integration	28
7.2	Machine learning for Wilson coefficient determination	28

7.3	Fitting inside the charmonium veto window	29
7.4	$B \rightarrow K^* \tau^+ \tau^-$ prospects	29
7.5	Adding other $b \rightarrow s \ell^+ \ell^-$ final states	29
8	Conclusions	30

1 Executive summary

Flavor-changing neutral current (FCNC) processes in the weak interaction do not occur at tree-level in the Standard Model (SM), which makes them sensitive probes of physics beyond the standard model (BSM). Intriguing BSM hints have been observed in $b \rightarrow s$ transitions by multiple flavor physics experiments, LHCb, Belle, BaBar, and Belle II. Here we investigate the prospects for the decay $B \rightarrow K^* \ell^+ \ell^-$ with $\ell = e, \mu$. We have implemented a new Monte Carlo (MC) signal generator inside the widely used event generator framework **EvtGen** [1], with improved SM decay amplitudes implemented in the operator product expansion in terms of the Wilson Coefficients C_7, C_9, C_{10} and their right-handed counterparts C'_7, C'_9, C'_{10} . Amplitudes for additional BSM physics contributions to $B \rightarrow K^* \ell \ell$, which we call $\delta C_i = C_i^{\text{eff}} - C_i^{\text{SM}}$, and which correspond to a general BSM signal resulting from dimension-six operators, can be chosen by the user. Non-zero δC_9 and δC_{10} for the di-muon final state are preferred by theoretical fits to current data. This corresponds to lepton flavor violation in $b \rightarrow s$ transitions.

We describe the advantages and potential of the newly developed ‘Sibidanov Physics Generator’ in improving sensitivity of New Physics (NP) searches and clarifying NP signatures. We have examined potential experimental correlations in the four variables that characterize $B \rightarrow K^* \ell^+ \ell^-$ decays (Fig. 1): the invariant mass of the lepton pair, q^2 , the lepton helicity angle from the virtual Z/γ -decay, $\cos \theta_\ell$, the K^* helicity angle, $\cos \theta_K$, and the angle between the K^* and di-lepton decay planes, χ . In addition, there are angular asymmetries which are a function of q^2 .

Inclusion of NP in the generator allows one to properly simulate acceptance bias in BSM scenarios, interference between SM and BSM amplitudes, and correlations between different BSM observables. For example, δC_9 will lead to correlated signatures in the angular asymmetries A_{FB} versus q^2 and S_5 versus q^2 . However, the $d\Gamma/dq^2$ spectrum is unchanged by this NP in C_9 .

Another striking signature of C'_7 is found in the modulation of the angle χ at low q^2 in $B \rightarrow K^* e^+ e^-$. Belle II has excellent sensitivity to such NP in C_7 and C'_7 .

We show that exploiting such correlations between angular observables substantially improves experimental sensitivity. We describe the potential for improved measurements from the expected 50 ab^{-1} dataset of the Belle II experiment with four-dimensional, unbinned likelihood fits to $B \rightarrow K^* \ell^+ \ell^-$ observables.

The observed angular asymmetries could originate from SM QCD or $c\bar{c}$ resonance effects, which appear in the experimental final state $K^*\ell^+\ell^-$. Given the difficulties in reliably computing all of the possible hadronic effects, the use of Δ observables appears to be the only possible approach to definitively distinguish between these effects and establish NP in $b \rightarrow s\mu^+\mu^-$. Using the NP Monte Carlo generator, we will demonstrate the feasibility of this experimental approach using Δ -observables. The three most important observables are:

$$\Delta A_{\text{FB}}(B \rightarrow K^*\ell\ell) \equiv A_{\text{FB}}(B \rightarrow K^*\mu^+\mu^-) - A_{\text{FB}}(B \rightarrow K^*e^+e^-), \quad (1)$$

$$\Delta S_5(B \rightarrow K^*\ell\ell) \equiv S_5(B \rightarrow K^*\mu^+\mu^-) - S_5(B \rightarrow K^*e^+e^-), \quad (2)$$

and

$$\Delta C_9^{\text{eff}}(B \rightarrow K^*\ell\ell) \equiv C_9^{\text{eff}}(B \rightarrow K^*\mu^+\mu^-) - C_9^{\text{eff}}(B \rightarrow K^*e^+e^-). \quad (3)$$

An example of Δ -like variables was introduced in Ref. [2]. Belle has already made a first attempt to measure Δ -type observables in $B \rightarrow K^*\ell^+\ell^-$ using a 0.7 ab^{-1} data sample [3]. The Δ -observables appear ideally suited for Belle II (which has comparable sensitivities for di-electrons and di-muons) with the large data sets expected in the next decade [4].

2 Overview

2.1 Current experimental anomalies in $b \rightarrow s$ neutral current (FCNC) processes

The tensions with the SM observed in the LFU violating ratios R_K and R_K^* by the LHCb collaboration are now at the 3.1σ [5] and $2.1\sigma - 2.4\sigma$ [6] significance level, respectively, in the low dilepton mass-squared region. However, measurements from the BaBar [7] and Belle [8, 9] collaborations are currently compatible with the SM expectation albeit with limited statistics. A similar pattern of deviations (although statistically not very significant) are also observed in two other LFU violating ratios $R_{K_S^0}$ and $R_{K^{*+}}$ [10]. Furthermore, there are significant deviations from SM expectations observed in angular asymmetries of $B \rightarrow K^*\mu^+\mu^-$ [11] and $B_s \rightarrow \phi\mu^+\mu^-$ [12] decays.

Several theoretical groups fit all $b \rightarrow s\ell\ell$ observables (R_K type results and angular asymmetries) for NP Wilson coefficients, δC_i in $b \rightarrow s\mu^+\mu^-$ and suggest a coherent picture of New Physics in C_9 and C_{10} [13, 14, 15, 16]. NP in δC_9 and δC_{10} is found with a significance of up to 5σ , though this varies by global analysis.

In order to explain the R_K deviation, the global fits assume that the NP is restricted to the di-muon channel and does not affect the di-electron channel. This is plausible if the NP is lepton-mass dependent. These claims for NP in $b \rightarrow s$ have stimulated a great deal of excitement in High Energy Physics.

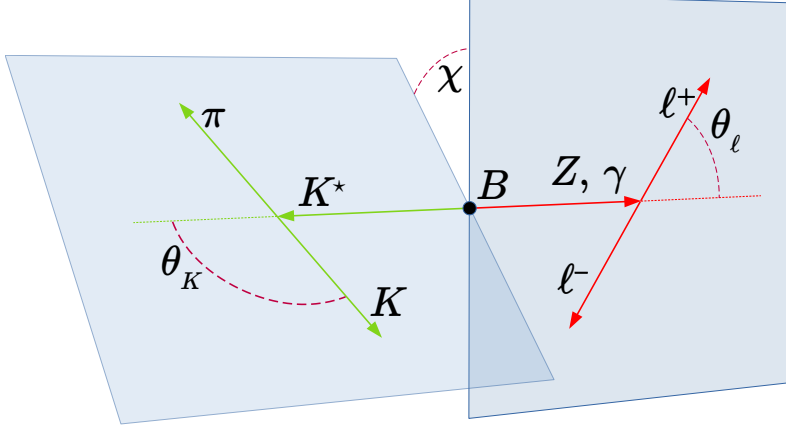


Figure 1: The $B \rightarrow K^*\ell^+\ell^-$ decay and the subsequent $K^* \rightarrow K\pi$ decay kinematic parameters.

2.2 Definition of observables and angular asymmetries

For the $B \rightarrow K^*\ell^+\ell^-$ decay with $K^* \rightarrow K\pi$ the differential decay rate can be described in terms of the $K\pi$ invariant mass $m_{K\pi}$, the di-lepton mass squared q^2 , and three angles θ_ℓ , θ_K , and χ . The angle θ_ℓ is defined as the angle between the direction of the positively charged lepton and the direction of B meson in the di-lepton rest frame. The angle θ_K is defined as the angle between the direction of the kaon and the direction of the B meson in the K^* -meson rest frame. The angle χ is the angle between the plane formed by the di-lepton pair and the plane formed by the K^* decay products in the B -meson rest frame. A graphical representation of the angle definitions is shown in Fig. 1.

In the SM angular asymmetries such as A_{FB} arise due to the interference between the photon and Z -boson contributions to the decay amplitude. In the case of NP there will be additional interference terms that are linear in the NP contribution, which appear in several observables to be discussed next. The well known forward-backward asymmetry $A_{\text{FB}}(q^2)$ is defined as

$$A_{\text{FB}}(q^2) = \frac{\left[\left(\int_0^1 - \int_{-1}^0 \right) d \cos \theta_\ell \right] d(\Gamma - \bar{\Gamma})}{\int_{-1}^1 d \cos \theta_\ell d(\Gamma + \bar{\Gamma})}, \quad (4)$$

where Γ and $\bar{\Gamma}$ denote the decay rate of $\bar{B}^0 \rightarrow \bar{K}^{0*} \ell \ell$ and the CP -conjugate channel $B^0 \rightarrow K^{0*} \ell \ell$, respectively (see Eqs. 19 and 28 for full angular distributions). Other important angular asymmetries involve the angle χ between the K^* and di-lepton decay planes [17]:

$$S_4(q^2) = -\frac{\pi}{2} \frac{\left[\int_{-\pi/2}^{\pi/2} - \int_{\pi/2}^{3\pi/2} \right] d\chi \left[\int_0^1 - \int_{-1}^0 \right] d \cos \theta_K \left[\int_0^1 - \int_{-1}^0 \right] d \cos \theta_\ell d(\Gamma + \bar{\Gamma})}{\int_0^{2\pi} d\chi \int_{-1}^1 d \cos \theta_K \int_{-1}^1 d \cos \theta_\ell d(\Gamma + \bar{\Gamma})}, \quad (5)$$

and

$$S_5(q^2) = \frac{4}{3} \frac{\left[\int_{-\pi/2}^{\pi/2} - \int_{\pi/2}^{3\pi/2} \right] d\chi \left[\int_0^1 - \int_{-1}^0 \right] d\cos\theta_K \int_{-1}^1 d\cos\theta_\ell d(\Gamma - \bar{\Gamma})}{\int_0^{2\pi} d\chi \int_{-1}^1 d\cos\theta_K \int_{-1}^1 d\cos\theta_\ell d(\Gamma + \bar{\Gamma})}. \quad (6)$$

Note that the angular observable P'_5 , widely used in the literature, is related to S_5 via $P'_5 \equiv S_5/\sqrt{F_L(1-F_L)}$, where F_L is the longitudinal polarization fraction of the K^* meson.

2.3 SM and candidate NP possibilities and their Lorentz structures

The starting point of our analysis is the following matrix element for the decay $B \rightarrow K^* \ell^+ \ell^-$:

$$\begin{aligned} \mathcal{M} = & \frac{G_F \alpha}{\sqrt{2}\pi} V_{tb} V_{ts}^* \left\{ \left[\langle K^* | \bar{s} \gamma^\mu (C_9^{\text{eff}} P_L + C'_9 P_R) b | \bar{B} \rangle \right. \right. \\ & - \frac{2m_b}{q^2} \langle K^* | \bar{s} i \sigma^{\mu\nu} q_\nu (C_7^{\text{eff}} P_R + C'_7 P_L) b | \bar{B} \rangle \left. \right] (\bar{\ell} \gamma_\mu \ell) \\ & + \langle K^* | \bar{s} \gamma^\mu (C_{10} P_L + C'_{10} P_R) b | \bar{B} \rangle (\bar{\ell} \gamma_\mu \gamma_5 \ell) \left. \right\}. \end{aligned} \quad (7)$$

where the SM Wilson coefficients are known at NNLL accuracy [18]:

$$\begin{aligned} C_7^{\text{eff}} &= -0.304, \\ C_9^{\text{eff}} &= C_9 + Y(q^2) = 4.211 + Y(q^2), \\ C_{10} &= -4.103, \end{aligned} \quad (8)$$

and where the function $Y(q^2)$ is described in Section 5. The chirality flipped operators $C'_{7,9,10}$ are highly suppressed in the SM but can arise in the presence of beyond the SM physics. Note that the SM Wilson coefficient C_9^{eff} varies with q^2 ; as shown in Fig. 2 separately for real and imaginary parts. We assume BSM states are heavy, far above the m_b scale. We therefore treat NP contributions to the Wilson coefficients as q^2 -independent shifts.

The $B \rightarrow K^*$ matrix elements in Eq. 7 can be expressed in terms of seven form factors that depend on the momentum transfer q^2 between the B and the K^* ($q^\mu = p^\mu - k^\mu$):

$$\begin{aligned} \langle \bar{K}^*(k) | \bar{s} \gamma_\mu (1 \mp \gamma_5) b | \bar{B}(p) \rangle = & \mp i \epsilon_\mu^* (m_B + m_{K^*}) A_1(q^2) \pm i (2p - q)_\mu (\epsilon^* \cdot q) \frac{A_2(q^2)}{m_B + m_{K^*}} \\ & \pm i q_\mu (\epsilon^* \cdot q) \frac{2m_{K^*}}{q^2} [A_3(q^2) - A_0(q^2)] + \epsilon_{\mu\nu\rho\sigma} \epsilon^{*\nu} p^\rho k^\sigma \frac{2V(q^2)}{m_B + m_{K^*}}, \end{aligned} \quad (9)$$

$$\text{with } A_3(q^2) = \frac{m_B + m_{K^*}}{2m_{K^*}} A_1(q^2) - \frac{m_B - m_{K^*}}{2m_{K^*}} A_2(q^2) \text{ and } A_0(0) = A_3(0); \quad (10)$$

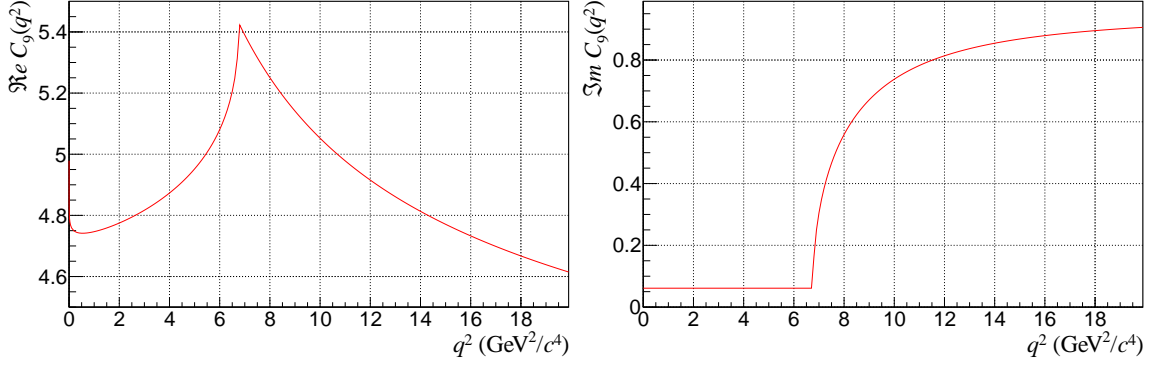


Figure 2: The SM Wilson coefficient C_9 versus q^2 now used in **EvtGen** (see Eq. 8) without $c\bar{c}$ resonances.

$$\begin{aligned} \langle \bar{K}^*(k) | \bar{s} \sigma_{\mu\nu} q^\nu (1 \pm \gamma_5) b | \bar{B}(p) \rangle &= i \epsilon_{\mu\nu\rho\sigma} \epsilon^{*\nu} p^\rho k^\sigma 2T_1(q^2) \\ &\pm T_2(q^2) [\epsilon_\mu^* (m_B^2 - m_{K^*}^2) - (\epsilon^* \cdot q) (2p - q)_\mu] \pm T_3(q^2) (\epsilon^* \cdot q) \left[q_\mu - \frac{q^2}{m_B^2 - m_{K^*}^2} (2p - q)_\mu \right] \end{aligned} \quad (11)$$

with $T_1(0) = T_2(0)$. Here ϵ_μ is the polarization vector of the K^* . We used the following convention for the Levi-Civita tensor $\epsilon_{0123} = +1$.

We adopt the formalism developed in Ref. [19] where the extrapolation of form factors from the calculated LCSR input points ($q^2 \lesssim 0$ GeV) to larger q^2 values is performed by a simple pole form with a z -expansion

$$F_i^{B \rightarrow K^*}(q^2) \equiv \frac{1}{1 - q^2/m_{R,i}^2} \sum_{n=0}^2 \alpha_n^i [z(q^2) - z(0)]^n, \quad (12)$$

where $z(t) \equiv \frac{\sqrt{t_+ - t} - \sqrt{t_+ - t_0}}{\sqrt{t_+ - t} + \sqrt{t_+ - t_0}}$, $t_\pm = (m_B \pm m_{K^*})^2$ and $t_0 \equiv t_+ (1 - \sqrt{1 - t_-/t_+})$.

The values for the fit parameters $\alpha_{0,1,2}^i$ including the correlation among them, and the masses of resonances $m_{R,i}$ associated with the quantum numbers of the respective form factor F_i are obtained in Ref. [19].

2.4 Form factor uncertainties

In the old **EvtGen** model BTOSLLBALL, used by Belle and Belle II up to now, the form factors were taken from Ref. [20]. In our new **EvtGen** model BTOSLLNP (see Section 2.5), we have now implemented the most recent hadronic form factors from Ref. [19], also known as the ABSZ form factor parameterization. ABSZ updates the previous computations by including current hadronic inputs and several theoretical improvements such as inclusion of higher twist distribution amplitudes of mesons, as well as a combined fit to Light-Cone Sum Rule form factors for the low q^2 region and Lattice QCD estimates valid in the high q^2 range. The form factor fit results are expressed as the coefficients of the expansion shown in Eq. 12.

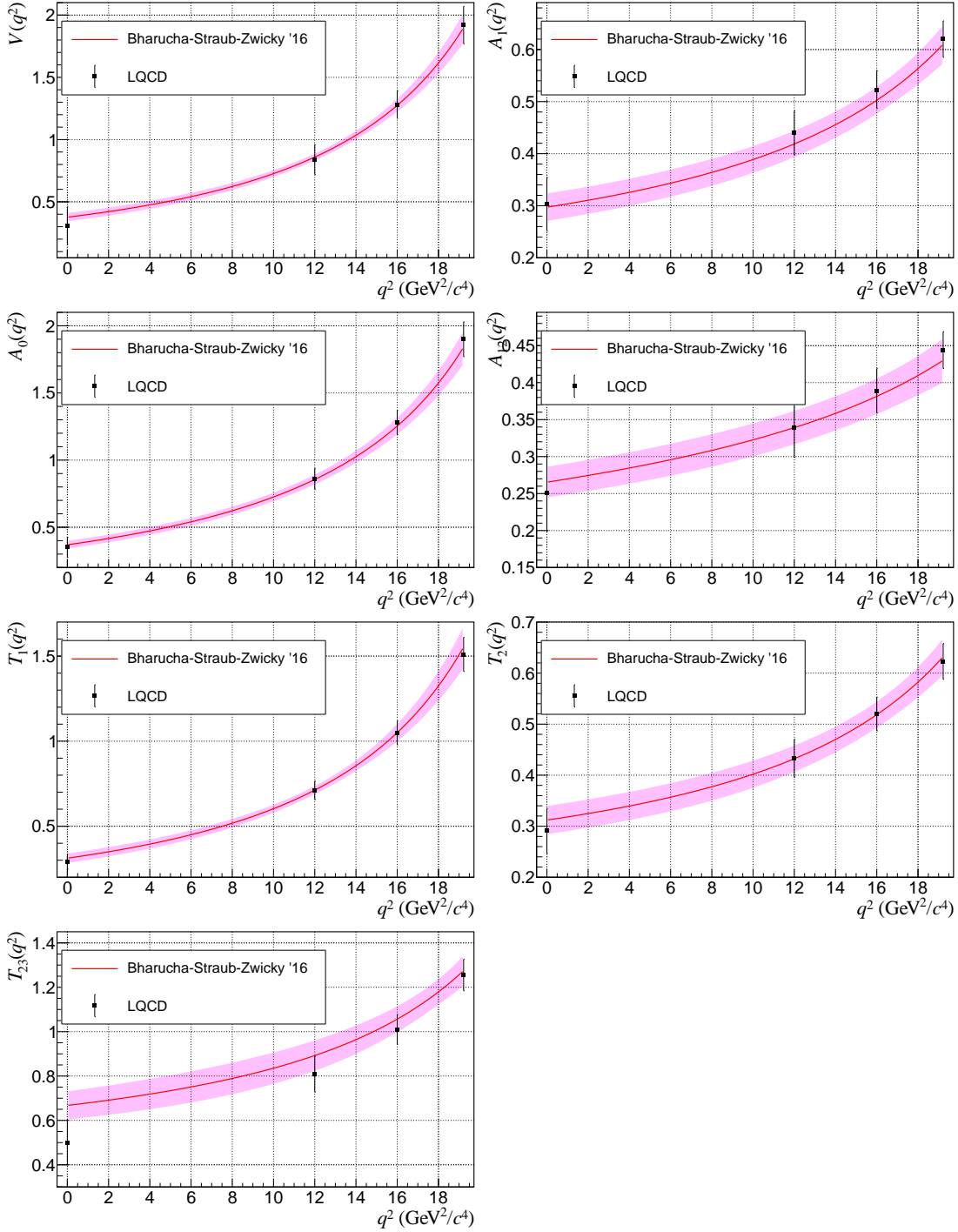


Figure 3: Result of the combined fit to LCSR and LQCD calculations from Ref. [19] for $B \rightarrow K^*$ hadronic form factors. The shaded bands show the combined one-standard-deviation uncertainty of the fit according the provided covariance matrix. The points with error bars show LQCD results from Table 11 in Ref. [21]. These theoretical uncertainties in the form factors can limit extraction of new physics.

There are seven form factors, which are functions of q^2 : $V(q^2)$, $A_0(q^2)$, $A_1(q^2)$, $A_2(q^2)$, $T_1(q^2)$, $T_2(q^2)$, and $T_3(q^2)$. In fact the form factors A_{12} and T_{23} are explicitly parameterized in Ref. [19], where the form factors A_2 and T_3 are extracted using the following expression:

$$A_{12}(q^2) = \frac{(m_B + m_{K\pi})^2(m_B^2 - m_{K\pi}^2 - q^2)A_1(q^2) - \lambda(q^2)A_2(q^2)}{16m_B m_{K\pi}^2(m_B + m_{K\pi})}, \quad (13)$$

and

$$T_{23}(q^2) = \frac{(m_B^2 - m_{K\pi}^2)^2(m_B^2 + 3m_{K\pi}^2 - q^2)T_2(q^2) - \lambda(q^2)T_3(q^2)}{8m_B m_{K\pi}^2(m_B - m_{K\pi})}. \quad (14)$$

Here $\lambda(q^2)$ is the Källén-function defined in Eq. 27 and $m_{K\pi}$ is the invariant mass of the kaon and pion to take into account the finite width of K^* . If the K^* width is omitted, a singularity appears in the physical region.

The resulting form factors we now use in **EvtGen** are shown in Figs. 3 and 4. Note that the theoretical uncertainties in the form factors shown in the figure limit extraction of new physics. Below, we discuss strategies for overcoming this limitation.

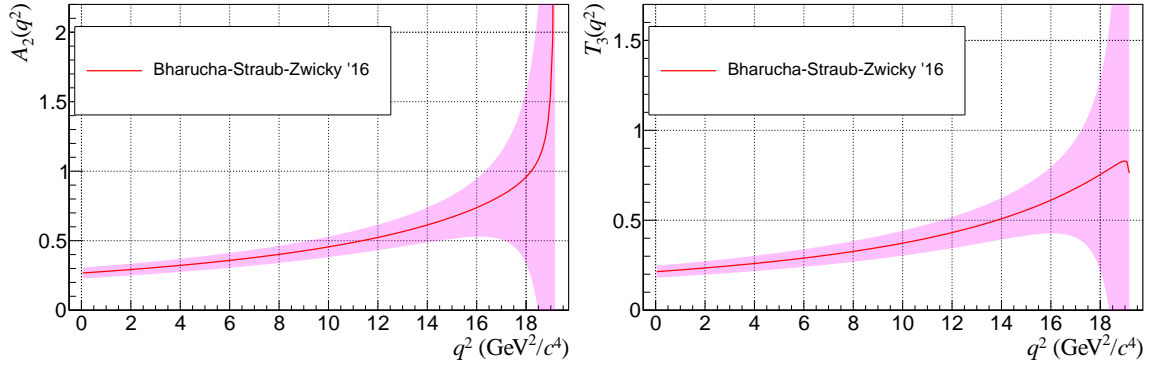


Figure 4: The $B \rightarrow K^*$ hadronic form factors A_2 and T_3 obtained using Eq. 13 and 14. The shaded bands show the propagated one-standard-deviation uncertainty. These theoretical uncertainties in the form factors can limit extraction of new physics.

2.5 Modifications to the EvtGen Monte Carlo Generator

We implement the $B \rightarrow K^* \ell^+ \ell^-$ generator with NP contributions in the **EvtGen** Monte-Carlo simulation framework. We use the BTOSLLBALL model as a reference to create the BTOSLLNP model, which incorporates the desired matrix element with NP. Here we use the generator, BTOSLLNP, only in the standalone mode but it has been also successfully integrated into the Belle II Analysis Software Framework (BASF2 [22]). In the model BTOSLLNP, the user can specify the following NP input parameters: δC_7 , C'_7 , δC_9 , C'_9 , δC_{10} , C'_{10} , $C_S - C'_S$, and $C_P - C'_P$. In the last two cases only such combinations are relevant. Each of these model parameters is complex-valued. The parameters can be specified in any order and in any combination in the user card. The default value for each parameter is zero and if no parameters are specified in the card the generator gives the SM result. Below we

present an example of a user decay card to illustrate the usage of the NP $B \rightarrow K^* \ell^+ \ell^-$ MC generator:

```
## the first argument is the Cartesian(0) or polar(1) representation of complex
## NP coefficients, which are three consecutive numbers
## {id, Re(C), Im(C)} or {coeff id, |C|, Arg(C)}

## id==0 delta C_7 -- NP addition to NNLO SM value
## id==1 delta C_9 -- NP addition to NNLO SM value
## id==2 delta C_10 -- NP addition to NNLO SM value
## id==3 C'_7 -- NP right-handed coefficient
## id==4 C'_9 -- NP right-handed coefficient
## id==5 C'_10 -- NP right-handed coefficient
## id==6 (C_S - C'_S) -- NP scalar left- and right-handed coefficient
## id==7 (C_P - C'_P) -- NP pseudo-scalar left- and right-handed coefficient

Decay anti-B0
## delta C_9eff = (-0.87, 0.0) all other coefficients correspond to the
## SM values
1.000 anti-K*0 e+ e- BTOSLLNP 0 1 -0.87 0.0 ;
Enddecay
```

To generate NP the user inputs several arguments in the user decay card as shown in the example above. The first argument specifies the coordinate system—Cartesian(0) or polar(1)—to be used for the complex-valued input arguments. The user can then enter each desired NP parameter as three consecutive numbers. These triplets can be entered in any order.

In the old BTOSLLBALL model used by Belle and Belle II, the form factors were taken from Ref. [20]. In the BTOSLLNP model, we have now implemented the most recent hadronic form factors from Ref. [19], also known as the ABSZ form factor parameterization, described above.

Besides adding the NP amplitudes and the ABSZ form factors to EvtGen, we also implemented a number of significant performance improvements, see Section 6.

3 Signatures of NP in $B \rightarrow K^* \ell^+ \ell^-$ and improved sensitivity via multi-dimensional likelihood fits

We show the expected sensitivity of the unbinned likelihood fit under ideal conditions using only the primary generator output without taking into account detector effects or hadronic uncertainties. Hadronic uncertainties are considered in Section 4.

A likelihood function has been implemented according to Eq. 19, where the matrix element defined in Eq. 7 is already squared, and which explicitly depends only on the four variables q^2 , $\cos \theta_\ell$, $\cos \theta_K$, χ , and on the Wilson coefficients as fit parameters. The likelihood function has been cross-checked against `EvtGen`-generated distribution and asymmetries. The quark masses $m_b = 4.8 \text{ GeV}/c^2$, $m_c = 1.3 \text{ GeV}/c^2$ were used. Good agreement between the `EvtGen` predictions and integrals of the likelihood function can be seen in Fig. 5.

The expected experimental data sample depends on integrated luminosity and on the selection criteria required to sufficiently suppress backgrounds. In Belle II, we currently expect about 20 to 30 % selection efficiency for the $B^0 \rightarrow K^{*0}(K^+ \pi^-) \ell^+ \ell^-$ mode and 40 to 50 fb^{-1} total integrated luminosity. Here we study only the statistical sensitivity of the fit so all internal parameters in the `EvtGen` decay generator and the likelihood function are the same. In addition, for simplicity we do not include resonance effects in the generator and the likelihood function and use the entire q^2 range without veto windows. The total decay rate is not fixed in the test. Depending on assumptions we expect from 5000 to 10000 events in the di-muon mode and about 25% more events at $q^2 \approx 0 \text{ GeV}^2/c^4$ for the di-electron mode. In the sensitivity tests below, the number of events lies within this range.

In each fit we extract the deviation of a single Wilson coefficient from the SM value:

$$\delta C_i = C_i^{\text{NP}} - C_i^{\text{SM}}.$$

Since the Wilson coefficients are complex numbers, both the real and imaginary parts are extracted in these fits, and shown in the figures that follow.

3.1 δC_9 correlated signatures in A_{FB} and S_5 (and $d\Gamma/dq^2$)

Figure 5 shows how the observables S_5 and A_{FB} are modified when a BSM contribution (δC_9) to C_9 is present. We assume that $\delta C_9 = -0.87$, which corresponds to a representative value from global theory fits to $b \rightarrow s$ experimental data in the $\mu\mu$ channel [13]. There are clear differences between the SM and BSM distributions of S_5 and A_{FB} , and these signatures are correlated. However, we do not see any significant effect of δC_9 on $d\Gamma/dq^2$.

Rather than the traditional method of performing binned fits to angular asymmetries in bins of q^2 , we now fit for δC_9 using 4D unbinned likelihood fits to q^2 , $\cos \theta_\ell$, $\cos \theta_K$, and χ with a δC_i as a free parameter. Fig. 6 shows the distribution of δC_9 resulting from pseudo-experiments performing such multidimensional fits repeatedly, assuming for now that $\delta C_9 = 0$ to check the sensitivity. According to the fit results the real and imaginary parts of C_9 can be constrained with a standard deviation of 0.15 and 0.35, corresponding

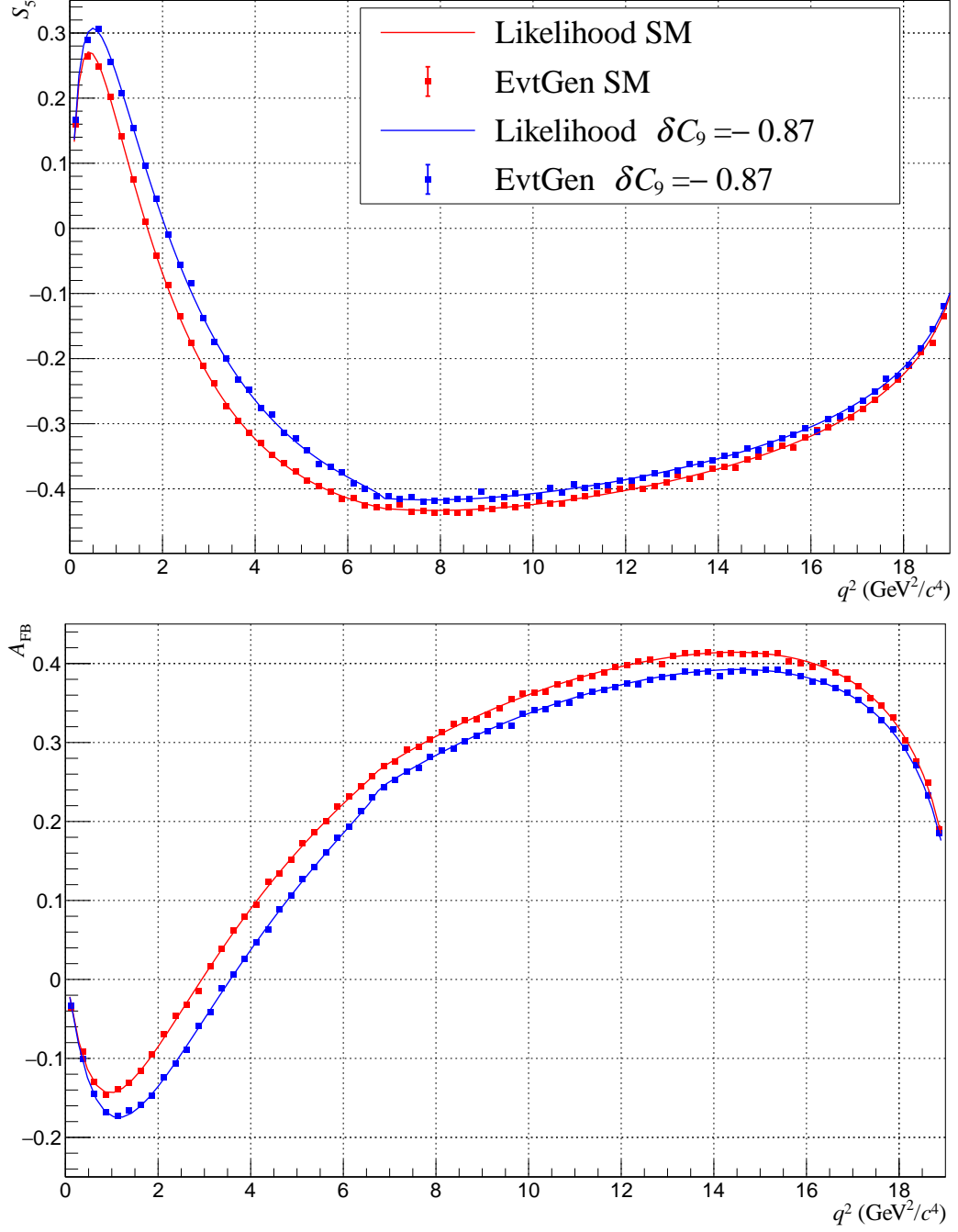


Figure 5: Comparison of S_5 (top plot) and A_{FB} (bottom plot) observables with NP $\delta C_9 = -0.87$ and SM $\delta C_9 = 0$ in the di-muon mode. The points are generated with the NP EvtGen simulation while the curves are the results of integrating the four-dimensional likelihood function.

to 3 and 7 % of $|C_9|$, respectively. This is a substantial improvement over the traditional method. The pull distributions demonstrate that the errors are correctly estimated in the fit procedure.

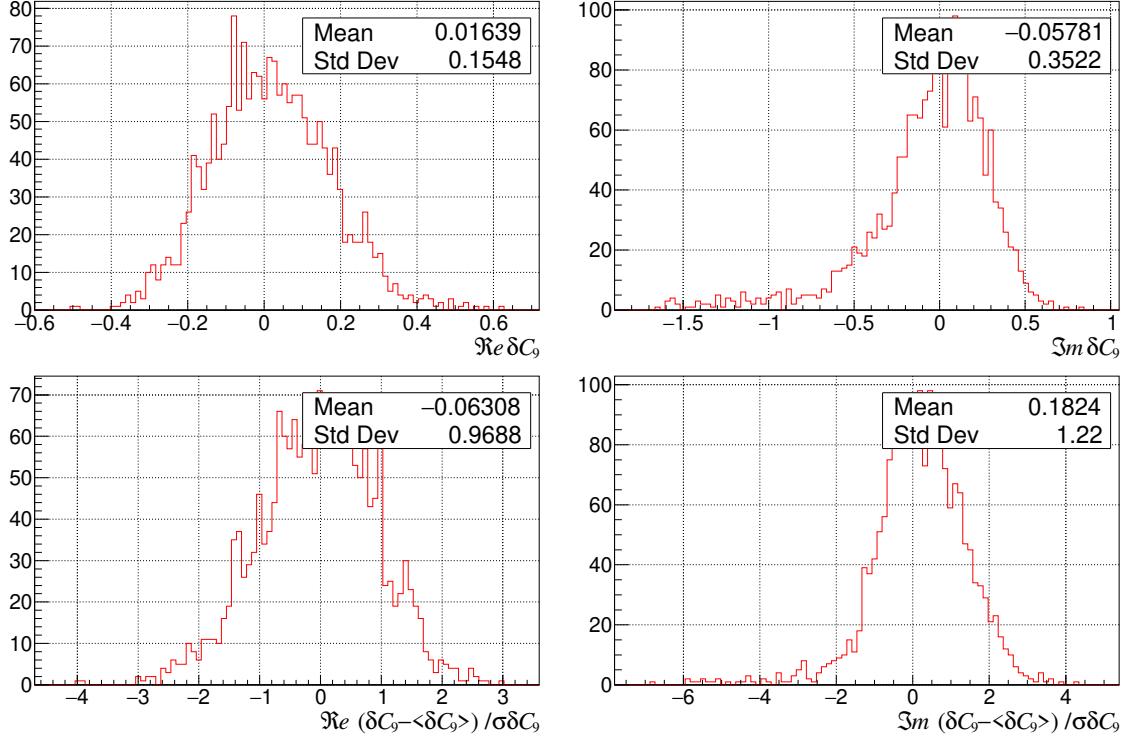


Figure 6: Distribution of δC_9 values obtained from unbinned likelihood fits to simulated $B \rightarrow K^* \mu^+ \mu^-$ SM decays in the full q^2 range, without resonances included. The real and imaginary parts of δC_9 extracted by the fits are shown in the top row. The bottom row shows the corresponding pull distributions, which demonstrate that the fitter correctly estimates fit uncertainties.

To further test the fit procedure we generate samples with the NP contribution $\delta C_9 = -0.87$ and repeat the multidimensional fits. The result is shown in Figs. 7 and 8 for the di-muon and di-electron modes, respectively. The fit extracts the real part of the NP contribution correctly with 8 and 10 standard deviation significance for the di-muon and di-electron modes, respectively. The imaginary part is consistent with zero and its uncertainty roughly matches to the SM fit results, albeit a small number of samples show relatively large deviation from zero – we will investigate what causes this behavior in the future.

3.2 δC_{10} sensitivity

In Fig. 9 the distribution of δC_{10} extracted from multidimensional fits is shown. According to the fit results the real and imaginary parts of δC_{10} can be constrained to 0.21 and 0.28,

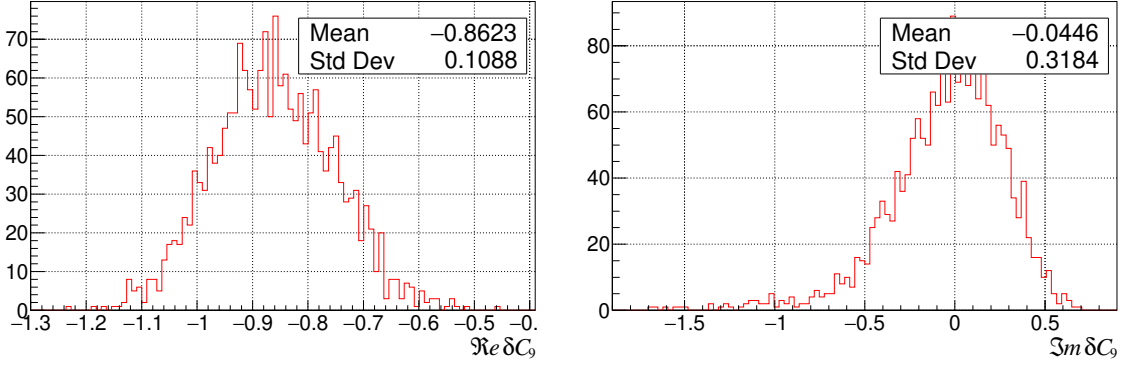


Figure 7: Distribution of δC_9 values obtained from unbinned likelihood fits to $B \rightarrow K^* \mu^+ \mu^-$ decays generated with the NP contribution $\delta C_9 = -0.87$ in the full q^2 range, without resonances included.

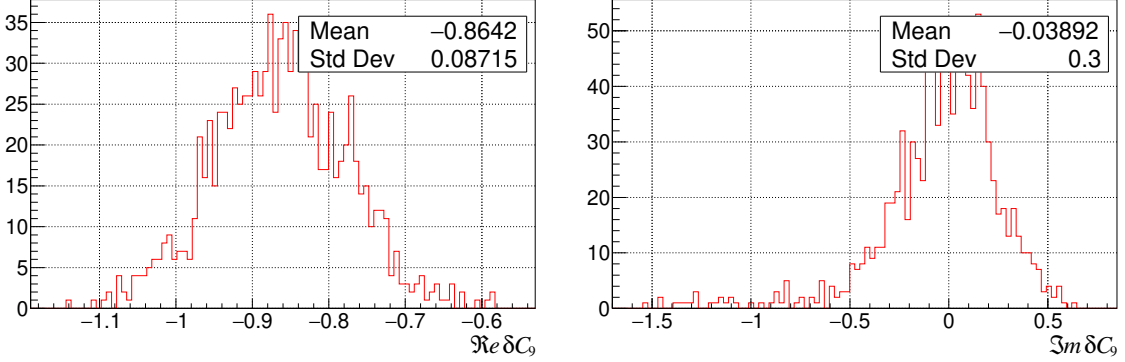


Figure 8: Distribution of δC_9 values obtained from unbinned likelihood fits to $B \rightarrow K^* e^+ e^-$ decays generated with the NP contribution $\delta C_9 = -0.87$ in the full q^2 range, without resonances included.

corresponding to 5 and 7 % of $|C_{10}| \approx 4.1$, respectively.

3.3 C'_9 and C'_{10} sensitivity

Next, we investigate the sensitivity to NP in the form of right-handed currents. The right-handed contribution C'_9 can be constrained at level of 3 % of $|C_9|$ in the di-muon mode as shown in Fig. 10. Similarly, the right-handed contribution C'_{10} should be constrained at level of 3 % of $|C_{10}|$ in the di-muon mode as shown in Fig. 11.

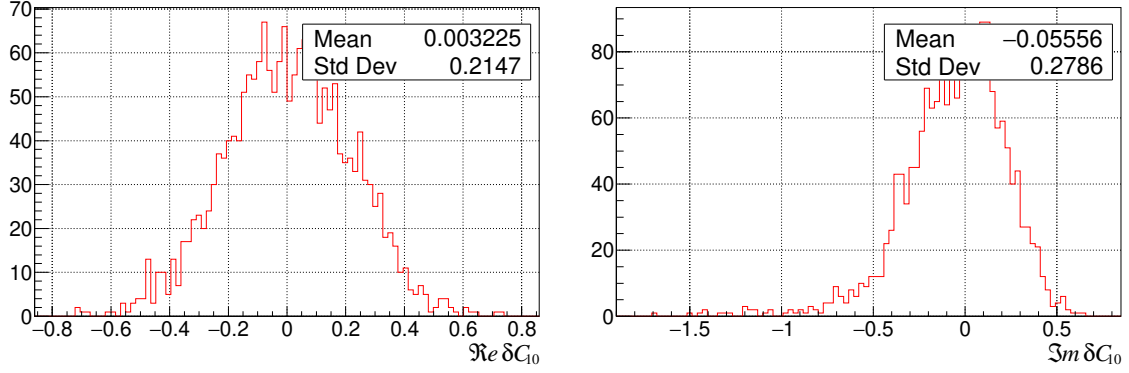


Figure 9: Distribution of δC_{10} values obtained from unbinned likelihood fits to simulated $B \rightarrow K^* \mu^+ \mu^-$ SM decays in the full q^2 range, without resonances included.

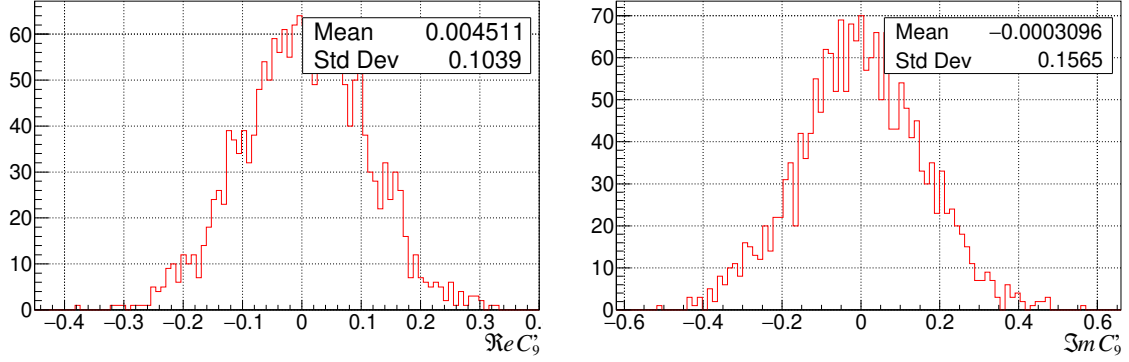


Figure 10: Distribution of C'_9 values obtained from unbinned likelihood fits to simulated $B \rightarrow K^* \mu^+ \mu^-$ SM decays in the full q^2 range, without resonances included.

3.4 C_7, C'_7 signatures at low q^2 and in the χ angle distribution

Sensitivity in the di-electron mode at low q^2 , $q^2 < 2 \text{ GeV}^2/c^4$, is critical as the new physics terms interfere with the photon pole. Even moderate non-zero C'_7 (right-handed NP) produces a prominent modulation in the χ distribution, while left-handed NP (δC_7) signatures appear at low q^2 and in the $\cos \theta_K$ distribution. These NP signatures are shown in Fig. 12.

In Fig. 13 the deviation δC_7 from the SM value of the corresponding Wilson coefficient is shown for the $B \rightarrow K^* \mu^+ \mu^-$ decay. The distribution of δC_7 shown in the top row behaves well – it is centered close to zero, relatively symmetric and has the normal distribution shape. The pull distribution shown in the bottom row also meets expectations with the average close to zero and standard deviation close to one, which indicates that the fit correctly estimates the statistical uncertainty. The SM NNLO value of $|C_7|$ is ≈ 0.3 so we expect to constrain the real and imaginary parts of C_7 to better than 2.5 and 7.5 %, respectively from

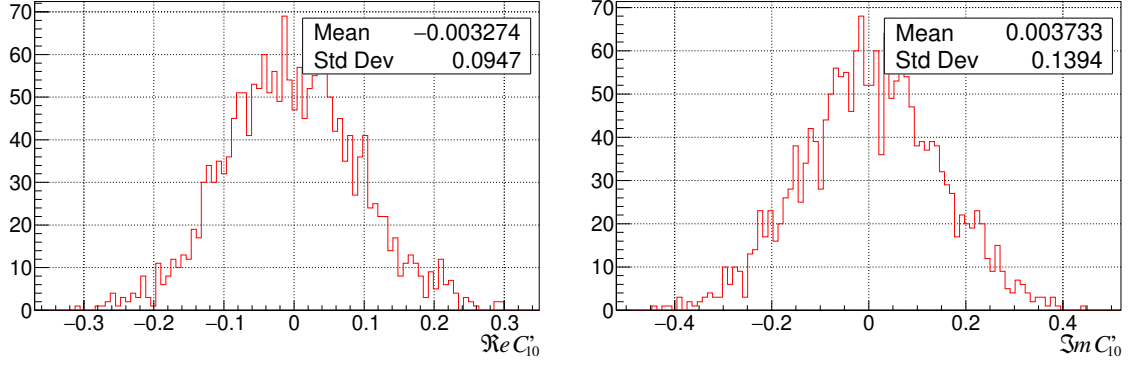


Figure 11: Distribution of C'_{10} values obtained from unbinned likelihood fits to simulated $B \rightarrow K^* \mu^+ \mu^-$ SM decays in the full q^2 range, without resonances included.

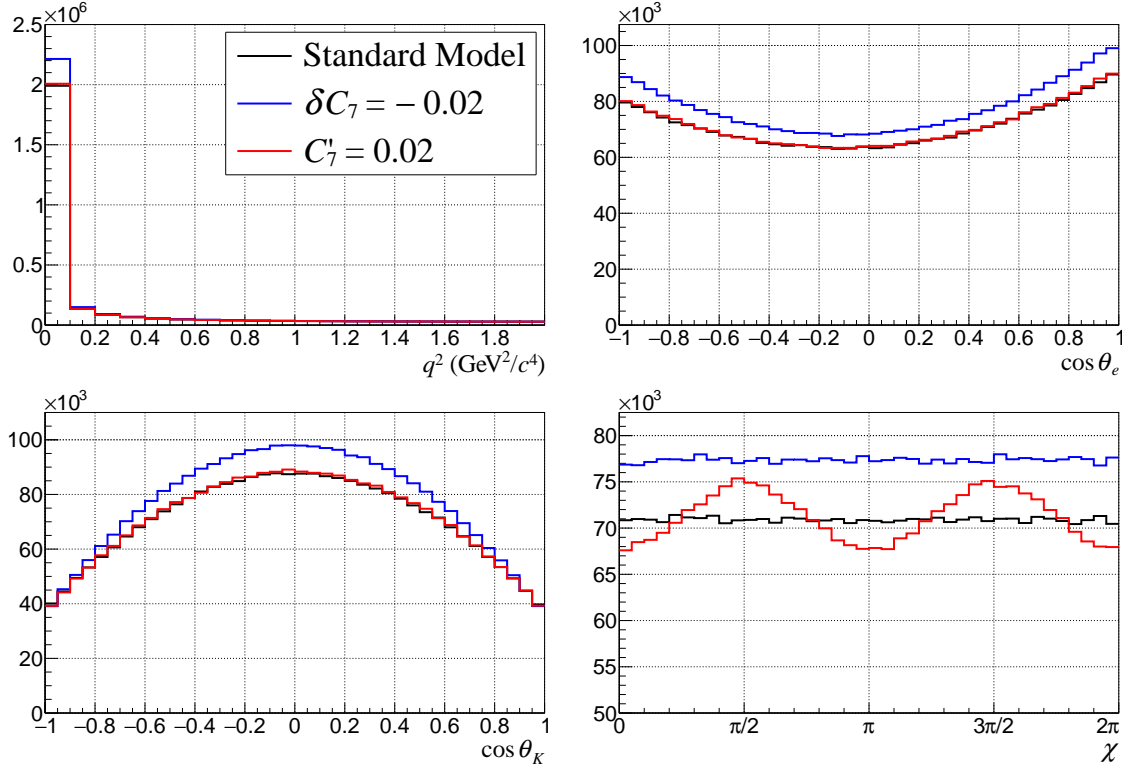


Figure 12: The effect of C'_7 and δC_7 on angular distributions in the di-electron decay mode for $q^2 < 2 \text{ GeV}^2/c^4$. There is a striking modulation in the χ angle distribution due to the right-handed NP contribution as well as clear left-handed NP signatures at low q^2 and in $\cos \theta_K$.

the di-muon mode alone. The contribution from NP in the form of right-handed currents, which corresponds to C'_7 , is expected to be constrained to better than 6 % of C_7 from the

di-muon mode alone, see Fig. 14. In the di-electron mode where we have access to the photon pole we will constrain the real and imaginary parts of C_7 to better than 1.5 and 6.5 %, respectively (Fig. 15) and C'_7 will be constrained to better than 3 % of $|C_7|$ (Fig. 16).

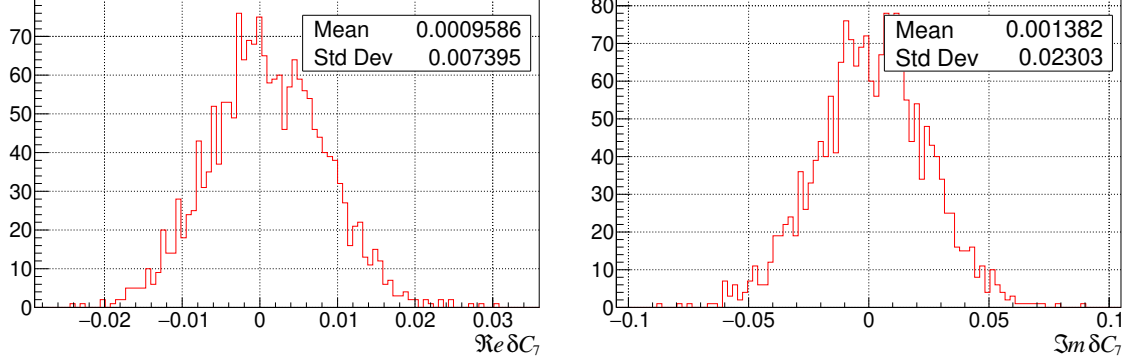


Figure 13: Distribution of δC_7 values obtained from unbinned likelihood fits to simulated $B \rightarrow K^* \mu^+ \mu^-$ SM decays in the full q^2 range, without resonances included.

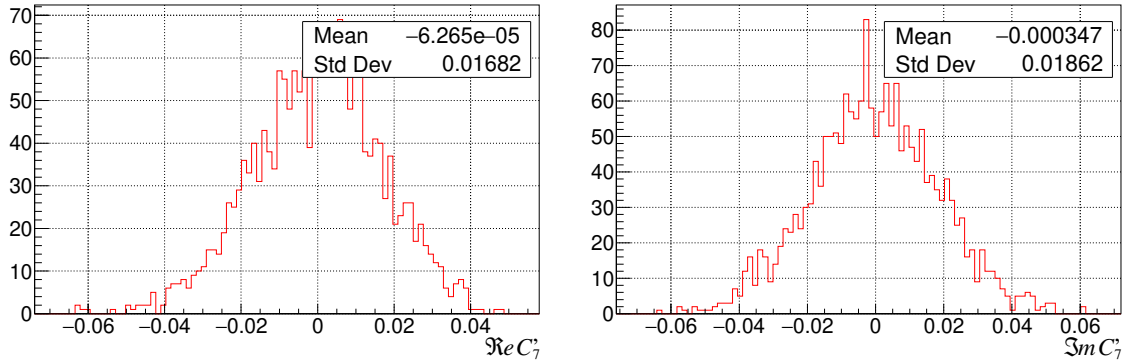


Figure 14: Distribution of C'_7 values obtained from unbinned likelihood fits to simulated $B \rightarrow K^* \mu^+ \mu^-$ SM decays in the full q^2 range, without resonances included.

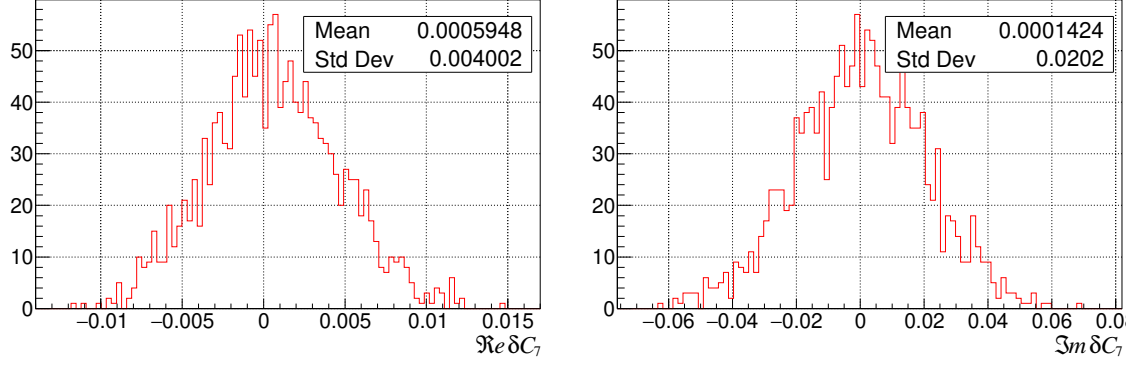


Figure 15: Distribution of δC_7 values obtained from unbinned likelihood fits to simulated $B \rightarrow K^* e^+ e^-$ SM decays in the full q^2 range, without resonances included.

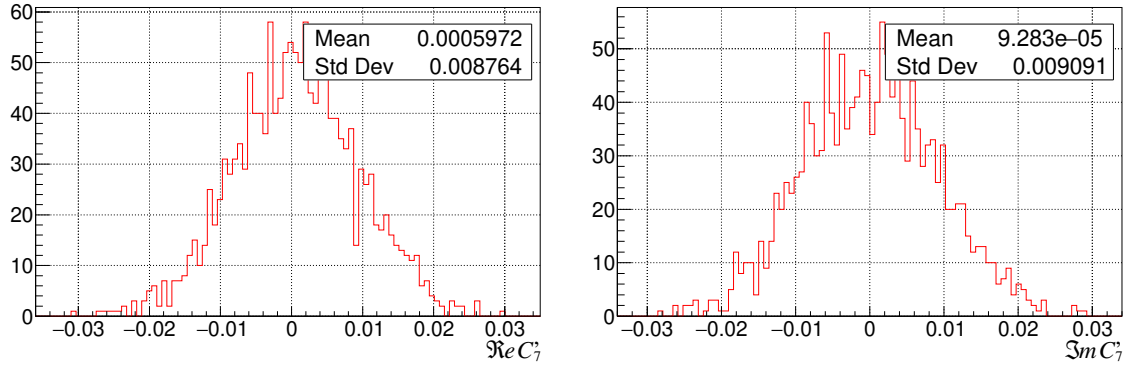


Figure 16: Distribution of C'_7 values obtained from unbinned likelihood fits to simulated $B \rightarrow K^* e^+ e^-$ SM decays in the full q^2 range, without including resonances.

4 How to disentangle QCD and resonance effects from NP in $B \rightarrow K^* \ell^+ \ell^-$

The semileptonic decays $B \rightarrow K^* \ell^+ \ell^-$ are expected to have smaller theoretical uncertainties than purely hadronic B decays. However, these decay modes still require QCD corrections, which are not easily calculable. As discussed above, the experimental final state $K^* \ell^+ \ell^-$ includes contributions from $c\bar{c}$ resonances such as $B \rightarrow J/\psi K^*$, $B \rightarrow \psi(2S) K^*$ as well as other broader $c\bar{c}$ resonances with higher mass, where the $c\bar{c}$ resonances decay to $\ell^+ \ell^-$. It is well known that these $b \rightarrow c\bar{c}s$ modes have non-factorizable contributions [23, 24, 25]. In addition, complications arise due to non-local contributions from electromagnetic corrections to purely hadronic operators [26], which cannot be calculated from first principles. Only limited success has been achieved in computing the effects of charm-loop contributions [27]. Given the difficulties in reliably computing all the QCD effects, our choice of Δ observables [4] offers the only existing approach to obtain sensitivity to NP.

The global fits assume that NP effects depend on lepton mass and are present in the muon mode but are negligible in the electron mode. This is required to explain the deviation in R_K and R_{K^*} from the SM. The SM hadronic uncertainties due to the strong interaction are the same in the both modes, and thus should cancel to first order in the difference so that only NP contributions remain.

We test the assumption that hadronic uncertainties affect the di-muon and di-electron modes equally, and cancel in the difference. We fit to pseudo-experiments with MC statistics roughly matched to the expectation for future Belle II experimental data. The MC data are generated using nominal ABSZ form factors [19]. In each fit the hadronic form factors in the unbinned likelihood function are varied, but taken to be the same for the di-muon and di-electron modes. Specifically, we randomly pick the parameters of the z -expansion within the uncertainties defined by the covariance matrices.

An example result is shown in Fig. 17 for the δC_9 variable, where a clear correlation between δC_9 extracted in the muon and electron modes is seen. The δC_9 distribution for the di-muon mode as well as the difference with the di-electron mode is shown in Fig. 18. The average value of the difference is close to zero and its standard deviation is about 40% less than for the di-muon mode alone and thus demonstrating the cancellation of hadronic uncertainties.

To illustrate the magnitude of possible bias on fitted Wilson coefficients from ABSZ hadronic form factor uncertainties, we again perform pseudo-experiments with form factor parameters in the likelihood function that differ from the nominal parameters used to generate the fitted MC data. This time, however, we use the same parameters for each fit, so that the bias does not average out over multiple experiments. In Fig. 19 the δC_9 coefficient extraction is shown as an example. We find that the systematic bias in this coefficient is nearly twice as large as the statistical uncertainty of the fit. With the expected amount of Belle II data, SM theoretical uncertainties might mimic NP effects.

Resonance effects are taken into account by modifying the Wilson coefficient C_9 according to Eq. 18 both in the `EvtGen` event generator and in the likelihood function. Figure 20

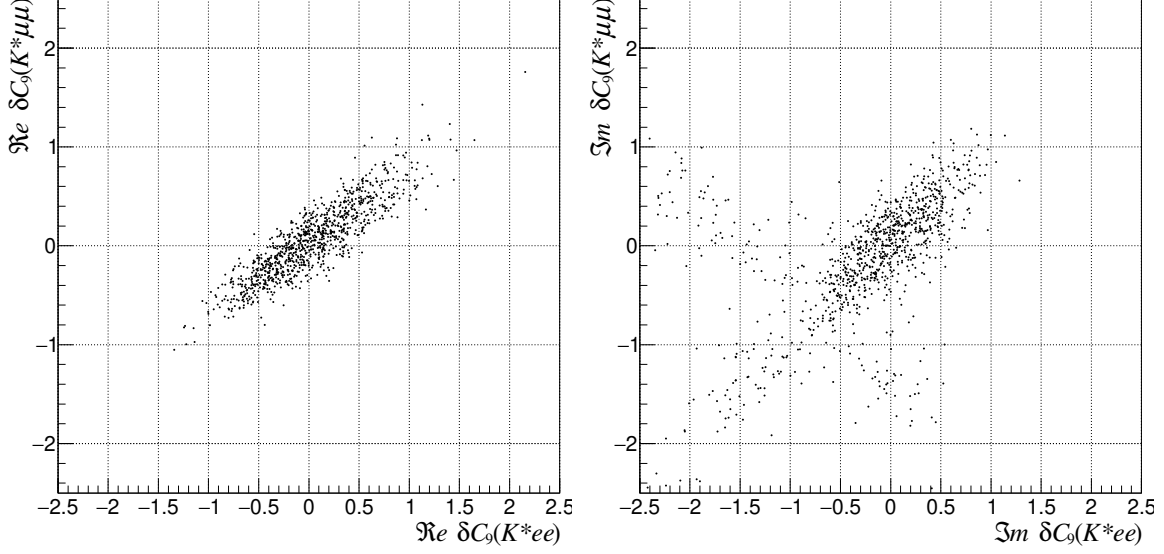


Figure 17: Result of 4-D unbinned likelihood fits for the δC_9 variable using both $B \rightarrow K^* e^+ e^-$ and $B \rightarrow K^* \mu^+ \mu^-$ MC data. Hadronic form factors are varied within their uncertainties. The fits are performed in the full q^2 range without resonances included. Note that the bias on the fitted δC_9 values, resulting from form factor uncertainties, is strongly correlated for the electron and muon modes.

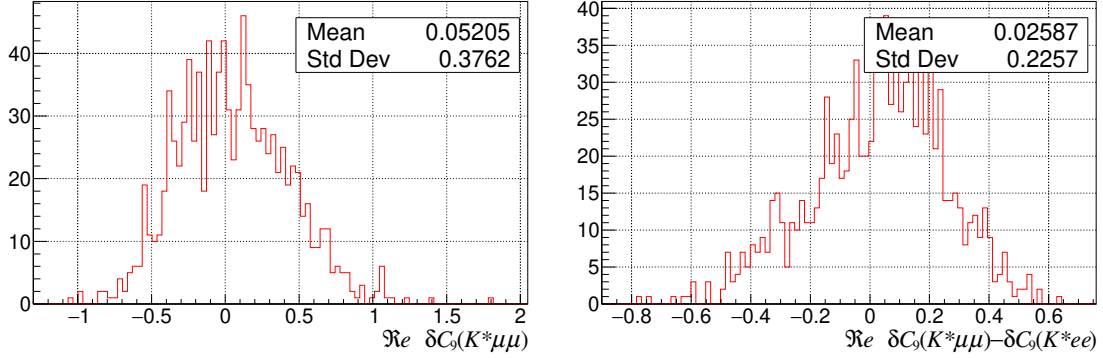


Figure 18: Distribution of the real part of the δC_9 coefficient obtained from fits to $B \rightarrow K^* \mu^+ \mu^-$ events (left plot) and the differences between those values and corresponding results for the $B \rightarrow K^* e^+ e^-$ mode (right plot) for randomly chosen hadronic form factors within the uncertainties as shown in Fig. 17. Note that uncertainties are reduced by subtracting the fit results for the two modes. The remaining uncertainty is due to limited statistics in each fit.

shows the q^2 distribution for $\overline{B} \rightarrow \overline{K}^* \mu^+ \mu^-$ decays. We find that resonances affect q^2 regions that extend well beyond the resonance widths, and thus rather large veto windows are required to mitigate their presence.

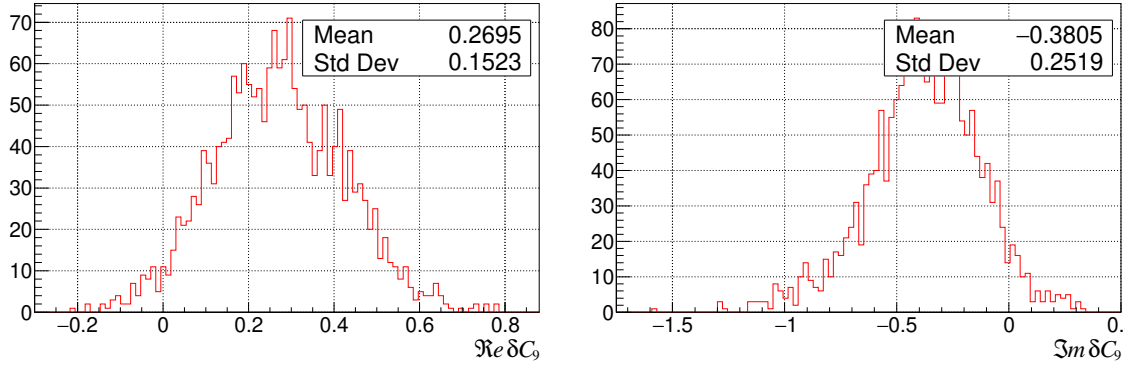


Figure 19: Distribution of δC_9 obtained from unbinned likelihood fits to simulated $B \rightarrow K^* \mu^+ \mu^-$ SM decays with a randomly selected but fixed set of 7 hadronic form factors, consistent with the SM within theoretical uncertainties. The shift of the mean (0.27 in $\text{Re } \delta C_9$) from zero cannot be distinguished from NP using this $B \rightarrow K^* \mu^+ \mu^-$ final state alone.

To illustrate how the resonances might affect the C_9 extraction even with large veto windows, we perform likelihood fits for the region $q^2 \in [1, 8] \cup [11, 12.5] \cup [15, q_{\text{max}}^2]$. For simplicity we use a likelihood function with two resonances only: J/ψ and $\psi(2S)$. SM MC data is generated without resonances. With the above q^2 selection applied, the average number of $K^* \mu^+ \mu^-$ and $K^* e^+ e^-$ decays in each fit is 4850. The total branching fraction is constrained with 5 % precision to the SM prediction. The results of the fits are shown in Fig. 21 (top row). The effect of the resonances is significant, biasing the fitted δC_9 values away from zero. This effect is particularly large for the imaginary part, where the bias is substantially larger than the SM value shown in Fig. 2. The Δ variables shown Fig. 21 (bottom row), however, behave well and are centered close to zero with uncertainties much smaller than the bias due to the resonances. This again suggests that possible NP contributions to the muon mode can be extracted even in the presence of large theoretical uncertainties by using Δ observables.

The remaining uncertainty then becomes statistical, rather than being limited by hadronic uncertainties. This highlights the importance of the technique utilizing the Δ variables, and the importance of large experimental statistics for both muon and electron modes.

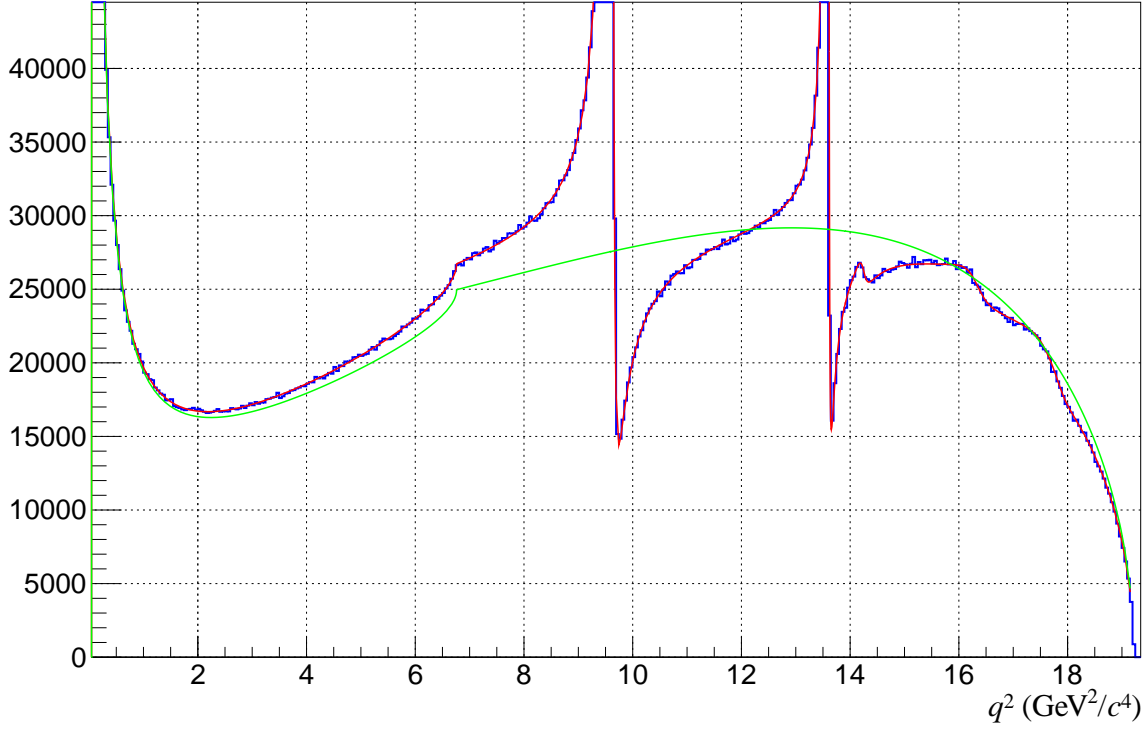


Figure 20: The q^2 distribution of $\bar{B} \rightarrow \bar{K}^* \mu^+ \mu^-$ decay in the presence of $c\bar{c}$ resonances. The histogram is the result from the **EvtGen** generator, the green curve shows the result of the likelihood integration without resonances, and the red curve is the result of the likelihood integration when resonances are included. The contribution of these resonances (and non-factorizable effects) will be a limiting uncertainty in the extraction of NP Wilson coefficients from $B \rightarrow K^* \mu^+ \mu^-$.

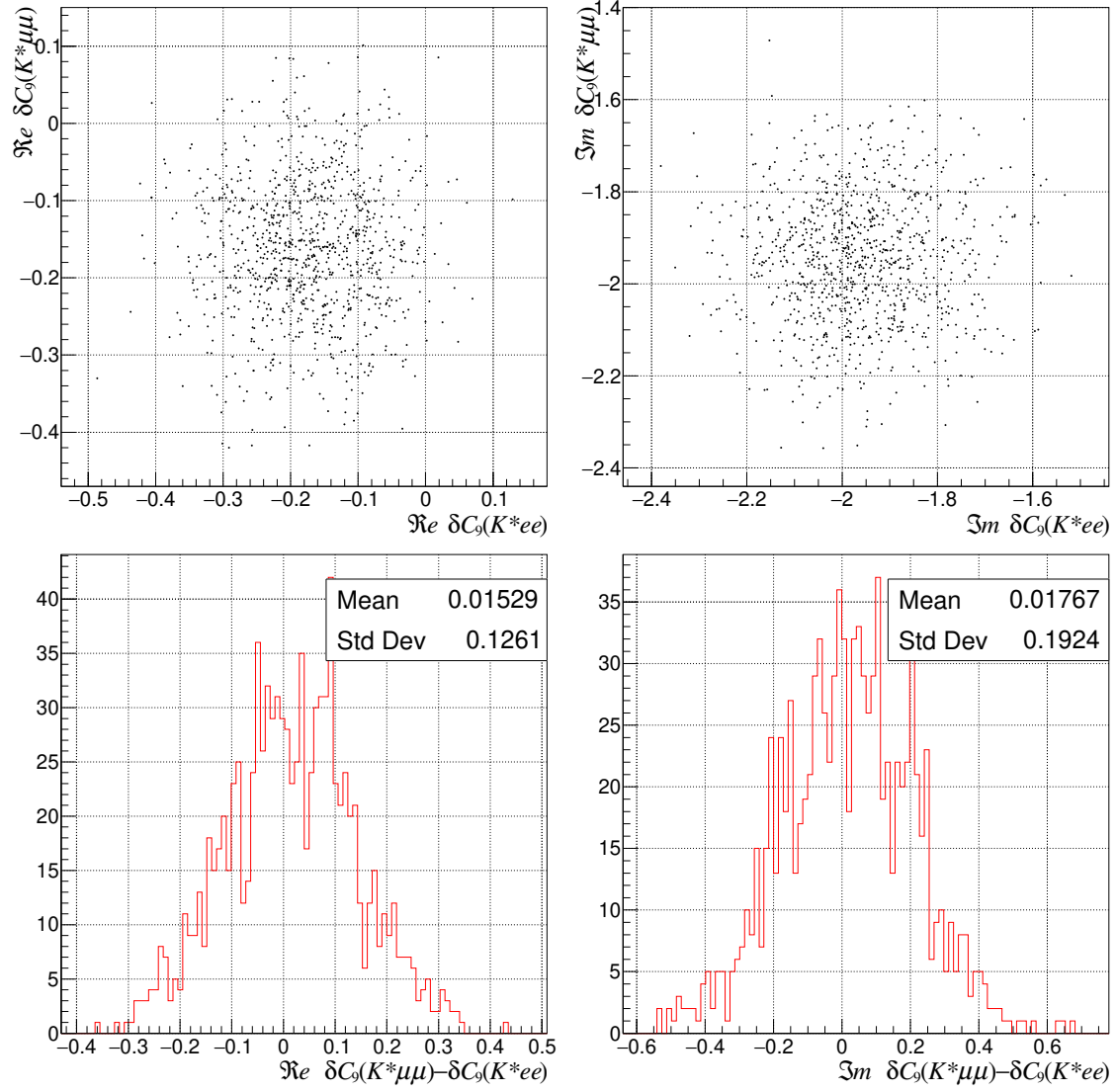


Figure 21: The test of the resonance effects in the fit on the δC_9 parameter. The top row shows correlation plots for the real and imaginary parts of δC_9 . The bottom row show the difference between modes.

5 Description of the theoretical framework

The matrix element introduced in Eq. 7 can further be extended via the inclusion of four dimension six operators namely

$$\mathcal{O}_S^{(\prime)} = (\bar{s}P_{R(L)}b)(\bar{\mu}\mu) \quad \text{and} \quad \mathcal{O}_P^{(\prime)} = (\bar{s}P_{R(L)}b)(\bar{\mu}\gamma_5\mu)$$

with the corresponding Wilson coefficients $C_S^{(\prime)}$ and $C_P^{(\prime)}$ which can arise in presence of NP. The SM prediction for C_i is known to NNLL accuracy and in the amplitude for $B \rightarrow K^*(\rightarrow K\pi)\ell^+\ell^-$ certain combinations of these Wilson coefficients appear, which are given by [18]

$$\begin{aligned} C_7^{\text{eff}} &= C_7 - \frac{1}{3}C_3 - \frac{4}{9}C_4 - \frac{20}{3}C_5 - \frac{80}{9}C_6, \\ C_9^{\text{eff}} &= C_9 + Y(q^2), \\ \text{with } Y(q^2) &= h(q^2, m_c) \left(\frac{4}{3}C_1 + C_2 + 6C_3 + 60C_5 \right) \\ &\quad - \frac{1}{2}h(q^2, m_b) \left(7C_3 + \frac{4}{3}C_4 + 76C_5 + \frac{64}{3}C_6 \right) \\ &\quad - \frac{1}{2}h(q^2, 0) \left(C_3 + \frac{4}{3}C_4 + 16C_5 + \frac{64}{3}C_6 \right) \\ &\quad + \frac{4}{3}C_3 + \frac{64}{9}C_5 + \frac{64}{27}C_6. \end{aligned} \quad (15)$$

The function

$$h(q^2, m_q) = -\frac{4}{9} \left(\ln \frac{m_q^2}{\mu^2} - \frac{2}{3} - z \right) - \frac{4}{9} (2+z) \sqrt{|z-1|} \times \begin{cases} \arctan \frac{1}{\sqrt{z-1}} & z > 1 \\ \ln \frac{1+\sqrt{1-z}}{\sqrt{z}} - \frac{i\pi}{2} & z \leq 1 \end{cases} \quad (16)$$

with $z = 4m_q^2/q^2$, is related to the basic fermion loop. The limiting function $h(q^2, 0)$ is given by

$$h(q^2, 0) = \frac{8}{27} + \frac{4}{9} \left(\ln \frac{\mu^2}{q^2} + i\pi \right). \quad (17)$$

One possible simplistic approach to include the resonance effects is to use a Breit-Wigner ansatz where the h function in Eq. 15 for the $c\bar{c}$ contributions should be replaced by [28]

$$h(m_c, q^2) \rightarrow h(m_c, q^2) - \frac{3\pi}{\alpha^2} \sum_{V=J/\psi, \psi', \dots} \frac{m_V \text{Br}(V \rightarrow \ell^+\ell^-) \Gamma_{\text{total}}^V}{q^2 - m_V^2 + im_V \Gamma_{\text{total}}^V}, \quad (18)$$

where m_V , Γ_{total}^V and Γ_{had}^V are the mass, total decay width and hadronic decay width of the vector boson V , respectively. Equation 18 assumes **no non-factorizable contributions**, and therefore no relative strong phase between the two terms. Using this approach C_9 is modified by the $c\bar{c}$ contributions as shown in Fig. 22.

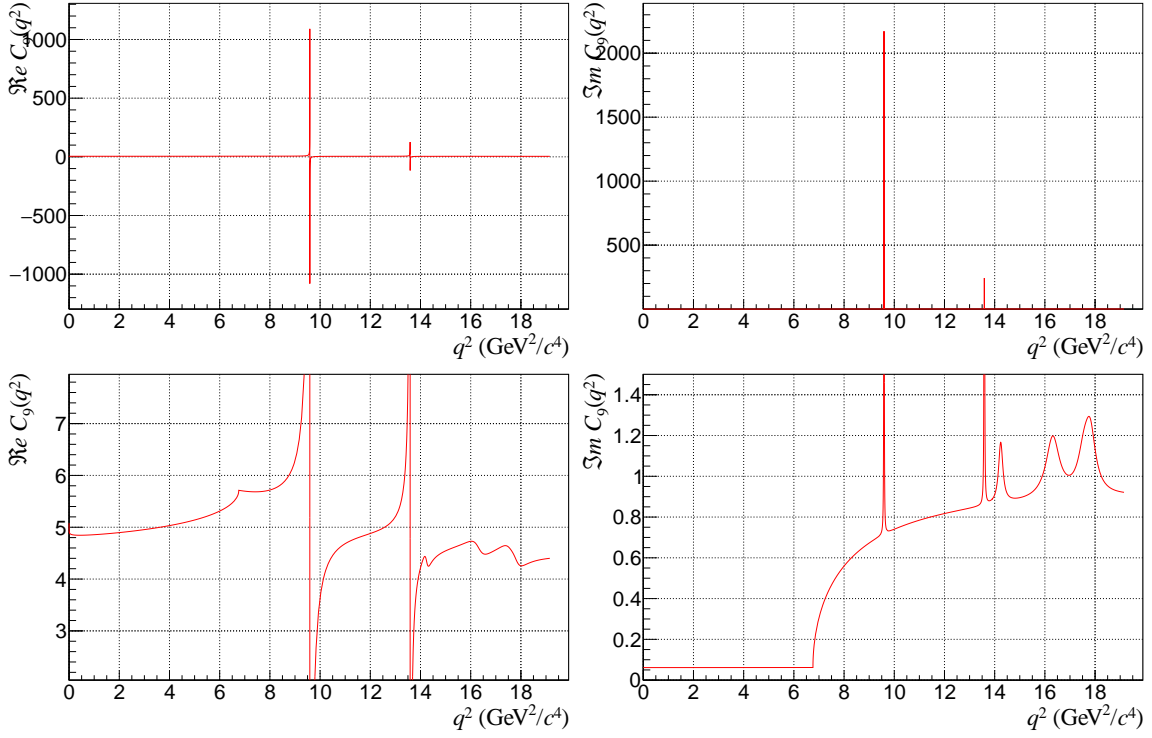


Figure 22: The SM Wilson coefficient C_9 versus q^2 (see Eq. 8) with $c\bar{c}$ resonances included. The top row shows the full range and the bottom row shows a zoomed-in version. The contribution of these resonances will be a limiting uncertainty in the extraction of NP Wilson coefficients from $B \rightarrow K^* \mu^+ \mu^-$.

The differential decay rate dependence on q^2 , $\cos \theta_\ell$, $\cos \theta_K$, and χ assuming zero-width K^* can be written as

$$\begin{aligned}
 \frac{d^4 \Gamma(\bar{B}^0 \rightarrow \bar{K}^{*0} \ell^+ \ell^-)}{dq^2 d\cos \theta_\ell d\cos \theta_K d\chi} &= I(q^2, \theta_\ell, \theta_K, \chi) = \\
 &= \frac{9}{32\pi} \left[I_1^s \sin^2 \theta_K + I_1^c \cos^2 \theta_K + (I_2^s \sin^2 \theta_K + I_2^c \cos^2 \theta_K) \cos 2\theta_\ell \right. \\
 &+ I_3 \sin^2 \theta_K \sin^2 \theta_\ell \cos 2\chi + I_4 \sin 2\theta_K \sin 2\theta_\ell \cos \chi + I_5 \sin 2\theta_K \sin \theta_\ell \cos \chi \\
 &+ I_6^s \sin^2 \theta_K \cos \theta_\ell + I_6^c \cos^2 \theta_K \cos \theta_\ell + I_7 \sin 2\theta_K \sin \theta_\ell \sin \chi \\
 &\left. + I_8 \sin 2\theta_K \sin 2\theta_\ell \sin \chi + I_9 \sin^2 \theta_K \sin^2 \theta_\ell \sin 2\chi \right]. \quad (19)
 \end{aligned}$$

The angular coefficients can be expressed in terms of transversity amplitudes as

$$I_1^s = \frac{(2 + \beta^2)}{4} \left[|\mathcal{A}_\perp^L|^2 + |\mathcal{A}_\parallel^L|^2 + (L \rightarrow R) \right] + \frac{4m^2}{q^2} \text{Re}(\mathcal{A}_\perp^L \mathcal{A}_\perp^{R*} + \mathcal{A}_\parallel^L \mathcal{A}_\parallel^{R*}), \quad (20a)$$

$$I_1^c = |\mathcal{A}_0^L|^2 + |\mathcal{A}_0^R|^2 + \frac{4m^2}{q^2} \left[|\mathcal{A}_t|^2 + 2\text{Re}(\mathcal{A}_0^L \mathcal{A}_0^{R*}) \right] + \beta^2 |\mathcal{A}_S|^2, \quad (20b)$$

$$I_2^s = \frac{\beta^2}{4} \left[|\mathcal{A}_\perp^L|^2 + |\mathcal{A}_\parallel^L|^2 + (L \rightarrow R) \right], \quad (20c)$$

$$I_2^c = -\beta^2 \left[|\mathcal{A}_0^L|^2 + (L \rightarrow R) \right], \quad (20d)$$

$$I_3 = \frac{\beta^2}{2} \left[|\mathcal{A}_\perp^L|^2 - |\mathcal{A}_\parallel^L|^2 + (L \rightarrow R) \right], \quad (20e)$$

$$I_4 = \frac{\beta^2}{\sqrt{2}} \left[\text{Re}(\mathcal{A}_0^L \mathcal{A}_\parallel^{L*}) + (L \rightarrow R) \right], \quad (20f)$$

$$I_5 = \sqrt{2}\beta \left[\text{Re}(\mathcal{A}_0^L \mathcal{A}_\perp^{L*}) - (L \rightarrow R) - \frac{m}{\sqrt{q^2}} \text{Re}(\mathcal{A}_\parallel^L A_S^* + \mathcal{A}_\parallel^R A_S^*) \right], \quad (20g)$$

$$I_6^s = 2\beta \left[\text{Re}(\mathcal{A}_\parallel^L \mathcal{A}_\perp^{L*}) - (L \rightarrow R) \right], \quad (20h)$$

$$I_6^c = 4\beta_\mu \frac{m_\mu}{\sqrt{q^2}} \text{Re} \left[\mathcal{A}_0^L A_S^* + (L \rightarrow R) \right], \quad (20i)$$

$$I_7 = \sqrt{2}\beta \left[\text{Im}(\mathcal{A}_0^L \mathcal{A}_\parallel^{L*}) - (L \rightarrow R) + \frac{m}{\sqrt{q^2}} \text{Im}(\mathcal{A}_\perp^L A_S^* + \mathcal{A}_\perp^R A_S^*) \right], \quad (20j)$$

$$I_8 = \frac{1}{\sqrt{2}}\beta^2 \left[\text{Im}(\mathcal{A}_0^L \mathcal{A}_\perp^{L*}) + (L \rightarrow R) \right], \quad (20k)$$

$$I_9 = \beta^2 \left[\text{Im}(\mathcal{A}_\parallel^{L*} \mathcal{A}_\perp^L) + (L \rightarrow R) \right], \quad (20l)$$

where

$$\beta = \sqrt{1 - \frac{4m^2}{q^2}}$$

and we have dropped the explicit q^2 dependence of the transversity amplitudes $\mathcal{A}_{\perp,\parallel,0}^{L,R}$ and \mathcal{A}_t for notational simplicity.

$$A_{\perp L,R} = N\sqrt{2}\lambda^{1/2} \left[\left[(C_9^{\text{eff}} + C_9^{\text{eff}'}) \mp (C_{10}^{\text{eff}} + C_{10}^{\text{eff}'}) \right] \frac{V(q^2)}{m_B + m_{K^*}} + \frac{2m_b}{q^2} (C_7^{\text{eff}} + C_7^{\text{eff}'}) T_1(q^2) \right], \quad (21)$$

$$A_{\parallel L,R} = -N\sqrt{2}(m_B^2 - m_{K^*}^2) \left[\left[(C_9^{\text{eff}} - C_9^{\text{eff}'}) \mp (C_{10}^{\text{eff}} - C_{10}^{\text{eff}'}) \right] \frac{A_1(q^2)}{m_B - m_{K^*}} + \frac{2m_b}{q^2} (C_7^{\text{eff}} - C_7^{\text{eff}'}) T_2(q^2) \right], \quad (22)$$

$$A_{0L,R} = -\frac{N}{2m_{K^*}\sqrt{q^2}} \left\{ \left[(C_9^{\text{eff}} - C_9^{\text{eff}'}) \mp (C_{10}^{\text{eff}} - C_{10}^{\text{eff}'}) \right] \times \left[(m_B^2 - m_{K^*}^2 - q^2)(m_B + m_{K^*})A_1(q^2) - \lambda \frac{A_2(q^2)}{m_B + m_{K^*}} \right] + 2m_b(C_7^{\text{eff}} - C_7^{\text{eff}'}) \left[(m_B^2 + 3m_{K^*}^2 - q^2)T_2(q^2) - \frac{\lambda}{m_B^2 - m_{K^*}^2} T_3(q^2) \right] \right\}, \quad (23)$$

$$A_t = \frac{N}{\sqrt{q^2}} \lambda^{1/2} \left[2(C_{10}^{\text{eff}} - C_{10}^{\text{eff}'}) + \frac{q^2}{m_\mu} (C_P - C'_P) \right] A_0(q^2), \quad (24)$$

$$A_S = -2N\lambda^{1/2} (C_S - C'_S) A_0(q^2), \quad (25)$$

where

$$N = V_{tb}V_{ts}^* \left[\frac{G_F^2 \alpha^2}{3 \cdot 2^{10} \pi^5 m_B^3} q^2 \lambda^{1/2} \beta \right]^{1/2}, \quad (26)$$

with

$$\lambda = \lambda(q^2) = m_B^4 + m_{K^*}^4 + q^4 - 2(m_B^2 m_{K^*}^2 + m_{K^*}^2 q^2 + m_B^2 q^2). \quad (27)$$

The differential distribution for the CP -conjugate mode $B^0 \rightarrow K^{0*} \ell \ell$ can be written as

$$\frac{d^4 \Gamma(B^0 \rightarrow K^{0*} \ell^+ \ell^-)}{dq^2 d\cos\theta_\ell d\cos\theta_K d\chi} = \bar{I}(q^2, \theta_\ell, \theta_K, \chi), \quad (28)$$

where $\bar{I}(q^2, \theta_\ell, \theta_K, \chi)$ is obtained with the following replacements in Eq. 19: $I_{1,2,3,4,7} \rightarrow \bar{I}_{1,2,3,4,7}$ and $I_{5,6,8,9} \rightarrow -\bar{I}_{5,6,8,9}$ [29]. Here I_i is equal to \bar{I}_i with all weak CP phases conjugated.

6 Signal generator performance improvements

In addition to implementing NP amplitudes and the ABSZ form factors in **EvtGen**, we also significantly improved the performance of **EvtGen**. The details of these improvements are briefly described below:

- The phase space generation procedure has been reviewed and significantly optimized.

- Tensor contraction operations have been reviewed and optimized.
- The importance sampling for three body decays with a pole has been reviewed and an incorrect treatment of the pole has been identified and fixed.
- The maximal amplitude search has been reviewed and several mistakes have been fixed.
- A special importance sampling procedure has been developed to treat narrow resonances for optimal performance.

Combining together all the **EvtGen** modifications more than two orders of magnitude performance improvement has been attained as shown in Fig. 23.

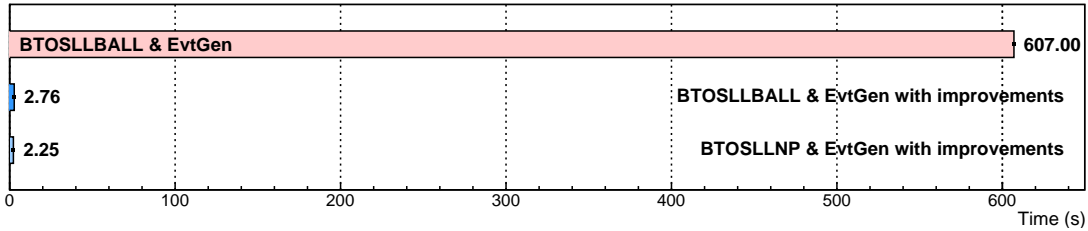


Figure 23: The measured time to generate 100000 $B \rightarrow K^* e^+ e^-$ events with (bottom bars) and without (top bar) **EvtGen** modifications.

7 Future work

7.1 Full MC simulation and EvtGen integration

Here we used the newly developed **EvtGen** model, BTOSLLNP, only in the standalone mode in order to identify NP signatures, but it has been also successfully integrated into the Belle II Analysis Software Framework (BASF2). We plan to simulate the full Belle II detector response including backgrounds and will update our sensitivities.

We are going to make the newly developed BTOSLLNP model, and the many additional improvements discussed above, part of the standard **EvtGen** distribution in the near future. These tools will then become publicly available.

7.2 Machine learning for Wilson coefficient determination

Machine learning algorithms can be used as a tool for parameter estimation where the likelihood is not known due to, among other things, the incorporation of detector effects and smearing [30]. Some of these methods and their implementation are described in Refs. [31, 32, 33, 34].

Novel to our proposal is to apply methods similar to those in Refs. [35] and [36] to Belle II datasets, to constrain NP signatures. Machine learning algorithms — such as neural networks (NNs), built using e.g. Keras [37] — can discriminate between SM and NP scenarios. For $B \rightarrow K^* \ell \ell$, we propose to train a NN using distributions of the variables q^2 , $\cos \theta_\ell$, $\cos \theta_K$, and χ , obtained from Monte Carlo simulations, to distinguish SM and NP scenarios. Alternatively, the A_{FB} and S_5 observables can be used to the same effect. The output layer of the NN can then be used with binned template fitting or other methods to estimate the sensitivity to the δC_i 's.

7.3 Fitting inside the charmonium veto window

To address non-factorizable contributions, we would like to fit the data inside the charmonium veto window(s) and constrain the strong phase of the SM $c\bar{c}$ contribution to the $K^* \ell^+ \ell^-$ final state.

7.4 $B \rightarrow K^* \tau^+ \tau^-$ prospects

The decay $B \rightarrow K^* \tau^+ \tau^-$ is potentially very sensitive to NP and can be also be generated with the new `EvtGen` model. The τ lepton decays to final states with missing neutrinos, which complicates complete reconstruction of its decays. We will study its NP signatures in the future.

7.5 Adding other $b \rightarrow s \ell^+ \ell^-$ final states

The NP sensitivities discussed here are statistics limited. Therefore, it is highly desirable to include additional final states.

One example is the use of $B \rightarrow K^* \ell \ell$ decays with $K^* \rightarrow K^0 \pi$. The $K^0 \rightarrow K_S$, $K_S \rightarrow \pi^+ \pi^-$ case is straightforward to fully reconstruct in the Belle II drift chamber. For the $K^0 \rightarrow K_L$ case, Belle II has a dedicated K_L and muon detector, but unfortunately, this detector can only measure the direction of the K_L , but not the magnitude of its momentum. There are sufficient kinematic constraints, however, to *calculate* this quantity, so that also these decays can be fully reconstructed. This basic idea has already been used successfully as part of the CP -violation measurements at Belle and BaBar, where $B \rightarrow J/\psi K_L$ decays were used together with $B \rightarrow J/\psi K_S$ to fit for $\sin 2\beta$ (a.k.a. $\sin 2\phi_1$). Including both K_S and K_L final states may substantially increase the $B \rightarrow K^* \ell \ell$ event statistics, however, the additional K_L signal will have somewhat lower purity, resulting from not measuring the magnitude of the K_L momentum. It has been proposed to upgrade the K_L -muon detector to measure K_L momenta via time-of-flight. If this proposal is adopted, the K_L final state may become as powerful as the K_S final state. Because backgrounds and detector performance are key issues here, we are planning further studies with full simulation.

8 Conclusions

We have upgraded the widely used MC event generator `EvtGen` to model $B \rightarrow K^* \ell^+ \ell^-$ with improved SM decay amplitudes and amplitudes for possible BSM physics contributions, implemented in the operator product expansion in terms of Wilson coefficients. This upgraded event generator has been used to investigate the signatures of the most general NP signal in $B \rightarrow K^* \ell^+ \ell^-$. We describe the advantages and potential of the newly developed ‘Sibidanov Physics Generator’ in improving sensitivity of New Physics searches and clarifying NP signatures. Advantages include properly simulating BSM scenarios, interference between SM and BSM amplitudes, and correlations between different BSM observables as well as acceptance bias. In addition to general improvements to `EvtGen`, we also improved the performance of `EvtGen` for $B \rightarrow K^* \ell^- \ell^+$ by two orders of magnitude by improving the treatment of the photon pole.

We have shown that exploiting correlations between angular observables substantially improves experimental sensitivity. The use of a four-dimensional unbinned maximum likelihood fit also dramatically improves sensitivity compared to traditional approaches with binned fits to angular asymmetries.

QCD uncertainties due to form factors and resonances now limit the sensitivity of fits for NP in $B \rightarrow K^* \ell^+ \ell^-$. We have described the feasibility of an approach using Δ -observables, which allow one to distinguish between hadronic effects and NP. The Δ -observables appear ideally suited for Belle II with the large, $\mathcal{O}(50 \text{ ab}^{-1})$, data sets expected in the next decade. For instance, δC_9 will be constrained to better than 3%. Belle II also has excellent sensitivity to NP in C_7 and C'_7 , which appear at low q^2 in the di-electron channel. For example, in the di-electron mode C'_7 will be constrained to 3% of C_7 .

ACKNOWLEDGEMENTS

T.E.B., S.D., S.K., A.S., and S.E.V. thank the DOE Office of High Energy Physics for support through DOE grant DE-SC0010504. The work of R.M. is supported by the University of Siegen under the Young Investigator Research Group (Nachwuchsforscherinnengruppe) grant.

References

- [1] D.J. Lange, *The EvtGen particle decay simulation package*, *Nucl. Instrum. Meth. A* **462** (2001) 152.
- [2] B. Capdevila, S. Descotes-Genon, J. Matias and J. Virto, *Assessing lepton-flavour non-universality from $B \rightarrow K^* \ell \ell$ angular analyses*, *JHEP* **10** (2016) 075 [[1605.03156](#)].

- [3] BELLE collaboration, *Lepton-Flavor-Dependent Angular Analysis of $B \rightarrow K^* \ell^+ \ell^-$* , *Phys. Rev. Lett.* **118** (2017) 111801 [[1612.05014](#)].
- [4] BELLE-II collaboration, *The Belle II Physics Book*, *PTEP* **2019** (2019) 123C01 [[1808.10567](#)].
- [5] LHCb collaboration, *Test of lepton universality in beauty-quark decays*, [2103.11769](#).
- [6] LHCb collaboration, *Test of lepton universality with $B^0 \rightarrow K^{*0} \ell^+ \ell^-$ decays*, *JHEP* **08** (2017) 055 [[1705.05802](#)].
- [7] BABAR collaboration, *Measurement of Branching Fractions and Rate Asymmetries in the Rare Decays $B \rightarrow K^{(*)} \ell^+ \ell^-$* , *Phys. Rev. D* **86** (2012) 032012 [[1204.3933](#)].
- [8] BELLE collaboration, *Test of lepton flavor universality and search for lepton flavor violation in $B \rightarrow K \ell \ell$ decays*, *JHEP* **03** (2021) 105 [[1908.01848](#)].
- [9] BELLE collaboration, *Measurement of the Differential Branching Fraction and Forward-Backward Asymmetry for $B \rightarrow K^{(*)} \ell^+ \ell^-$* , *Phys. Rev. Lett.* **103** (2009) 171801 [[0904.0770](#)].
- [10] LHCb collaboration, *Tests of lepton universality using $B^0 \rightarrow K_S^0 \ell^+ \ell^-$ and $B^+ \rightarrow K^{*+} \ell^+ \ell^-$ decays*, [2110.09501](#).
- [11] LHCb collaboration, *Measurement of CP-Averaged Observables in the $B^0 \rightarrow K^{*0} \mu^+ \mu^-$ Decay*, *Phys. Rev. Lett.* **125** (2020) 011802 [[2003.04831](#)].
- [12] LHCb collaboration, *Branching Fraction Measurements of the Rare $B_s^0 \rightarrow \phi \mu^+ \mu^-$ and $B_s^0 \rightarrow f_2'(1525) \mu^+ \mu^-$ Decays*, *Phys. Rev. Lett.* **127** (2021) 151801 [[2105.14007](#)].
- [13] W. Altmannshofer and P. Stangl, *New physics in rare B decays after Moriond 2021*, *Eur. Phys. J. C* **81** (2021) 952 [[2103.13370](#)].
- [14] M. Algueró, B. Capdevila, S. Descotes-Genon, J. Matias and M. Novoa-Brunet, *$b \rightarrow s \ell \ell$ Global Fits after R_{K_S} and $R_{K^{*+}}$* , 4, 2021 [[2104.08921](#)].
- [15] T. Hurth, F. Mahmoudi, D.M. Santos and S. Neshatpour, *More indications for lepton nonuniversality in $b \rightarrow s \ell^+ \ell^-$* , *Phys. Lett. B* **824** (2022) 136838 [[2104.10058](#)].
- [16] M. Ciuchini, M. Fedele, E. Franco, A. Paul, L. Silvestrini and M. Valli, *New Physics without bias: Charming Penguins and Lepton Universality Violation in $b \rightarrow s \ell^+ \ell^-$ decays*, [2110.10126](#).
- [17] R. Mandal, R. Sinha and D. Das, *Testing New Physics Effects in $B \rightarrow K^* \ell^+ \ell^-$* , *Phys. Rev. D* **90** (2014) 096006 [[1409.3088](#)].
- [18] W. Altmannshofer, P. Ball, A. Bharucha, A.J. Buras, D.M. Straub and M. Wick, *Symmetries and Asymmetries of $B \rightarrow K^* \mu^+ \mu^-$ Decays in the Standard Model and Beyond*, *JHEP* **01** (2009) 019 [[0811.1214](#)].

- [19] A. Bharucha, D.M. Straub and R. Zwicky, $B \rightarrow V\ell^+\ell^-$ in the Standard Model from light-cone sum rules, *JHEP* **08** (2016) 098 [[1503.05534](#)].
- [20] P. Ball and R. Zwicky, $B_{d,s} \rightarrow \rho, \omega, K^*, \phi$ decay form-factors from light-cone sum rules revisited, *Phys. Rev. D* **71** (2005) 014029 [[hep-ph/0412079](#)].
- [21] R.R. Horgan, Z. Liu, S. Meinel and M. Wingate, Rare B decays using lattice QCD form factors, *PoS LATTICE2014* (2015) 372 [[1501.00367](#)].
- [22] BELLE-II FRAMEWORK SOFTWARE GROUP collaboration, The Belle II Core Software, *Comput. Softw. Big Sci.* **3** (2019) 1 [[1809.04299](#)].
- [23] BELLE collaboration, Measurements of branching fractions and decay amplitudes in $B \rightarrow J/\psi K^*$ decays, *Phys. Lett. B* **538** (2002) 11 [[hep-ex/0205021](#)].
- [24] BABAR collaboration, Measurement of decay amplitudes of $B \rightarrow J/\psi K^*, \psi(2S)K^*$, and $\chi_{c1}K^*$ with an angular analysis, *Phys. Rev. D* **76** (2007) 031102 [[0704.0522](#)].
- [25] LHCb collaboration, Measurement of the polarization amplitudes in $B^0 \rightarrow J/\psi K^*(892)^0$ decays, *Phys. Rev. D* **88** (2013) 052002 [[1307.2782](#)].
- [26] M. Beneke, T. Feldmann and D. Seidel, Systematic approach to exclusive $B \rightarrow V\ell^+\ell^-$, $V\gamma$ decays, *Nucl. Phys. B* **612** (2001) 25 [[hep-ph/0106067](#)].
- [27] A. Khodjamirian, T. Mannel, A.A. Pivovarov and Y.M. Wang, Charm-loop effect in $B \rightarrow K^{(*)}\ell^+\ell^-$ and $B \rightarrow K^*\gamma$, *JHEP* **09** (2010) 089 [[1006.4945](#)].
- [28] F. Kruger and L.M. Sehgal, Lepton polarization in the decays $B \rightarrow X_s\mu^+\mu^-$ and $B \rightarrow X_s\tau^+\tau^-$, *Phys. Lett. B* **380** (1996) 199 [[hep-ph/9603237](#)].
- [29] F. Kruger, L.M. Sehgal, N. Sinha and R. Sinha, Angular distribution and CP asymmetries in the decays $\bar{B} \rightarrow K^-\pi^+e^-e^+$ and $\bar{B} \rightarrow \pi^-\pi^+e^-e^+$, *Phys. Rev. D* **61** (2000) 114028 [[hep-ph/9907386](#)].
- [30] J. Brehmer, Simulation-based inference in particle physics, *Nature Reviews Physics* **3** (2021) 305.
- [31] P. Baldi et al., Parameterized neural networks for high-energy physics, *The European Physical Journal C* **76** (2016) .
- [32] J. Brehmer et al., Constraining effective field theories with machine learning, *Phys. Rev. Lett.* **121** (2018) 111801.
- [33] J. Brehmer et al., A guide to constraining effective field theories with machine learning, *Phys. Rev. D* **98** (2018) 052004.
- [34] J. Brehmer et al., Mining gold from implicit models to improve likelihood-free inference, *Proceedings of the National Academy of Sciences* **117** (2020) 5242 [<https://www.pnas.org/doi/pdf/10.1073/pnas.1915980117>].

- [35] J. D'Hondt et al., *Learning to pinpoint effective operators at the LHC: a study of the $t\bar{t}b\bar{b}$ signature*, *Journal of High Energy Physics* **2018** (2018) .
- [36] N. Tonon et al., *Probing effective field theory operators in the associated production of top quarks with a Z boson in multilepton final states at $\sqrt{s} = 13$ TeV*, *Journal of High Energy Physics* **2021** (2021) .
- [37] F. Chollet et al., “Keras.” <https://keras.io>, 2015.